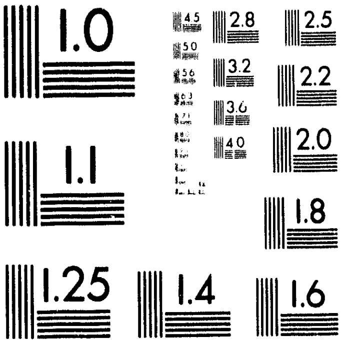
1.0
4.5
5.0
5.6
6.3
7.1
8.0
2.8
3.2
3.6
4.0
2.5
2.2
2.0
1.1
1.8
1.25
1.4
1.6

# 1 of 1

NUREG/CR-4667
ANL-93/27
Vol. 16
R5

# Environmentally Assisted Cracking in Light Water Reactors

## Semiannual Report
## October 1992—March 1993

Manuscript Completed: August 1993
Date Published: September 1993

Prepared by
H. M. Chung, O. K. Chopra, W. E. Ruther, T. F. Kassner,
W. F. Michaud, J. Y. Park, J. E. Sanecki, W. J. Shack

Argonne National Laboratory
9700 South Cass Avenue
Argonne, IL 60439

**Prepared for**
**Division of Engineering**
**Office of Nuclear Regulatory Research**
**U.S. Nuclear Regulatory Commission**
**Washington, DC 20555-0001**
**NRC FIN A2212**

## Previous Documents in Series

*Environmentally Assisted Cracking in Light Water Reactors Semiannual Report April—September 1985*, NUREG/CR-4667 Vol. I, ANL-86-31 (June 1986).

*Environmentally Assisted Cracking in Light Water Reactors Semiannual Report October 1985—March 1986*, NUREG/CR-4667 Vol. II, ANL-86-37 (September 1987).

*Environmentally Assisted Cracking in Light Water Reactors Semiannual Report April—September 1986*, NUREG/CR-4667 Vol. III, ANL-87-37 (September 1987).

*Environmentally Assisted Cracking in Light Water Reactors Semiannual Report October 1986—March 1987*, NUREG/CR-4667 Vol. IV, ANL-87-41 (December 1987).

*Environmentally Assisted Cracking in Light Water Reactors Semiannual Report April—September 1987*, NUREG/CR-4667 Vol. V, ANL-88-32 (June 1988).

*Environmentally Assisted Cracking in Light Water Reactors Semiannual Report October 1987—March 1988*, NUREG/CR-4667 Vol. 6, ANL-89/10 (August 1989).

*Environmentally Assisted Cracking in Light Water Reactors Semiannual Report April—September 1988*, NUREG/CR-4667 Vol. 7, ANL-89/40 (March 1990).

*Environmentally Assisted Cracking in Light Water Reactors Semiannual Report October 1988—March 1989*, NUREG/CR-4667 Vol. 8, ANL-90/4 (June 1990).

*Environmentally Assisted Cracking in Light Water Reactors Semiannual Report April—September 1989*, NUREG/CR-4667 Vol. 9, ANL-90/48 (March 1991).

*Environmentally Assisted Cracking in Light Water Reactors Semiannual Report October 1989—March 1990*, NUREG/CR-4667 Vol. 10, ANL-91/5 (March 1991).

*Environmentally Assisted Cracking in Light Water Reactors Semiannual Report April—September 1990*, NUREG/CR-4667 Vol. 11, ANL-91/9 (May 1991).

*Environmentally Assisted Cracking in Light Water Reactors Semiannual Report October 1990—March 1991*, NUREG/CR-4667 Vol. 12, ANL-91/24 (August 1991).

*Environmentally Assisted Cracking in Light Water Reactors Semiannual Report April—September 1991*, NUREG/CR-4667 Vol. 13, ANL-92/6 (March 1992).

*Environmentally Assisted Cracking in Light Water Reactors Semiannual Report October 1991—March 1992*, NUREG/CR-4667 Vol. 14, ANL-92/30 (August 1992).

*Environmentally Assisted Cracking in Light Water Reactors Semiannual Report April—September 1992*, NUREG/CR-4667 Vol. 15, ANL-93/2 (June 1993).

# Environmentally Assisted Cracking in Light Water Reactors

by

H. M. Chung, O. K. Chopra, W. E. Ruther, T. F. Kassner,
W. F. Michaud, J. Y. Park, J. E. Sanecki, and W. J. Shack

## Abstract

This report summarizes work performed by Argonne National Laboratory on fatigue and environmentally assisted cracking (EAC) in light water reactors (LWRs) during the six months from October 1992 to March 1993. Fatigue and EAC of piping, pressure vessels, and core components in LWRs are important concerns as extended reactor lifetimes are envisaged. Topics that have been investigated include (1) fatigue of low-alloy steel used in piping, steam generators, and reactor pressure vessels, (2) EAC of cast stainless steels (SSs), (3) radiation-induced segregation and irradiation-assisted stress corrosion cracking of Type 304 SS after accumulation of relatively high fluence, and (4) EAC of low-alloy steels. Fatigue tests were conducted on medium-sulfur-content A106-Gr B piping and A533-Gr B pressure vessel steels in simulated PWR water and in air. Additional crack growth data were obtained on fracture-mechanics specimens of cast austenitic SSs in the as-received and thermally aged conditions and chromium-nickel-plated A533-Gr B steel in simulated boiling-water reactor (BWR) water at 289°C. The data were compared with predictions based on crack growth correlations for ferritic steels in oxygenated water and correlations for wrought austenitic SS in oxygenated water developed at ANL and rates in air from Section XI of the ASME Code. Microchemical and microstructural changes in high- and commercial-purity Type 304 SS specimens from control-blade absorber tubes and a control-blade sheath from operating BWRs were studied by Auger electron spectroscopy and scanning electron microscopy.

## Contents

## Figures

## Tables

# Executive Summary

*Fatigue of Ferritic Piping and Pressure Vessel Steels*

Plain carbon steels are used extensively in PWR and BWR nuclear steam supply systems as piping and pressure vessel materials. The steels of interest for these applications include A106-Gr B and A333-Gr 6 for seamless pipe and A302-Gr B, A508-2, and A533-Gr B plate for pressure vessels. Additional fatigue tests were conducted on medium-sulfur-content A106-Gr B piping and A533-Gr B pressure vessel steels in simulated PWR water and in air. The fatigue life of A533-Gr B steel in deoxygenated water is generally shorter by a factor of 2 than that in air. No significant effect of the aqueous environments was observed in tests on A106-Gr B steel. The effects of load shape and loading rate will be further explored in subsequent testing.

*Environmentally Assisted Cracking of Cast Stainless Steels*

Additional crack growth rate (CGR) tests have been conducted on fracture-mechanics specimens of CF-8, and CF-8M grades of cast stainless steel (SS) in as-received and thermally aged conditions to characterize environmental, loading, and material conditions that can produce susceptibility to stress corrosion cracking (SCC) in these steels. The CGRs in high-purity water containing 0.2 and 5-8 ppm dissolved oxygen were compared with predictions found in Section XI of the ASME code for wrought SS in air and with modified correlations for wrought SSs in water. The results indicate that the air curve is frequently nonconservative, but for the most part, the data are bounded by the modified correlations for wrought SSs in water at 289°C. Thermal aging increases the yield and ultimate strengths of the steels, and the CGRs in water tend to increase with the square of the yield stress of the materials.

*Irradiation-Assisted Stress Corrosion Cracking of Type 304 SS*

Failures of austenitic SS after accumulation of high fluence have been attributed to radiation-induced segregation (RIS) or depletion of elements such as Si, P, S, Ni, and Cr. However, the exact identity of the elements that segregate and the degree to which RIS produces susceptibility of the core internal components of LWRs to irradiation-assisted SCC are unclear. Slow-strain-rate tensile (SSRT) tests and grain boundary analyses by Auger electron spectroscopy (AES) were conducted on high- and commercial-purity (HP and CP) Type 304 SS specimens from irradiated BWR components. Contrary to previous beliefs, susceptibility to intergranular stress corrosion cracking (IGSCC) could not be correlated with RIS of impurities such as Si, P, C, or S, but a correlation was obtained with grain-boundary Cr concentration, indicating that Cr depletion plays a role. However, grain-boundary concentrations of Cr determined from presently available field-emission-gun/scanning-transmission electron microscopy/energy-dispersive-spectroscopy (FEG-STEM-EDS) and AES techniques are not accurate enough to clarify the importance of Cr depletion. Grain-boundary analyses were conducted on BWR neutron absorber tubes that were fabricated from two HP heats of Type 304 SS that had virtually identical chemical compositions and irradiated to similar fluence level but that exhibited a significant difference in susceptibility to IGSCC during SSRT tests. Grain-boundary concentrations of Cr, Ni, Si, P, S, and C of the resistant and susceptible heats were virtually identical.

However, grain boundaries of the resistant material contained a lower concentration of N and higher concentrations of B and Li than those of the susceptible material.

Boron is known to undergo thermal segregation to grain boundaries in austenitic SSs. Therefore, grain-boundary concentrations of B, and hence Li, could be influenced strongly by thermomechanical processes even if core internal components are fabricated from the same starting material. During slow cooling of thicker sections (e.g., BWR top guide), thermal segregation of B, and hence Li, is likely to be more pronounced. This will be conducive to suppression of IASCC under conditions of a similar thermal sensitization (i.e., Cr depletion). The present study indicates that a synergism between grain-boundary segregation of N and B impurities and transmutation by thermal neutrons to H and Li, respectively, plays an important role in IASCC. However, the relative importance of the roles of grain-boundary Cr depletion and the concentrations of N, B, and Li on grain boundaries is not yet clear.

*Stress Corrosion Cracking of Ferritic Steels*

Additional fracture-mechanics CGR tests have been performed on nonplated specimens of A106-Gr B and A533-Gr B steel and on a specimen of A533-Gr B plated with Ni-Cr. The effect of frequency on CGR was determined at a load ratio of 0.9 in HP oxygenated (≈200 ppb) water at 289°C. The CGRs for the Ni-Cr-plated A533-Gr B specimen were compared with predicted values from new correlations proposed for inclusion in Section XI of the ASME Boiler and Pressure Vessel Code. The observed CGRs were adequately bounded by the proposed ASME Section XI correlations.

# 1 Introduction

Fatigue and environmentally assisted cracking (EAC) of piping, pressure vessels, and core components in light water reactors (LWRs) are important concerns as extended reactor lifetimes are envisaged. The degradation processes in U.S. reactors include fatigue of austenitic stainless steel (SS) in emergency core cooling systems[*] and pressurizer surge line[**] piping in pressurized water reactors (PWRs), intergranular stress corrosion cracking (IGSCC) of austenitic SS piping in boiling water reactors (BWRs), and propagation of fatigue or stress corrosion cracks (which initiate in sensitized SS cladding) into low-alloy ferritic steels in BWR pressure vessels.[***] Similar cracking has also occurred in upper-shell-to-transition-cone girth welds in PWR steam generator vessels,[+] and cracks have been found in steam generator feedwater distribution piping.[++] Occurrences of mechanical-vibration- and thermal-fluctuation-induced fatigue failures in LWR plants in Japan have also been documented.[1] Another concern is failure of reactor-core internal components after accumulation of relatively high fluence, which has occurred in both BWRs and PWRs. The general pattern of the observed failures indicates that as nuclear plants age and the neutron fluence increases, many apparently nonsensitized austenitic materials become susceptible to intergranular failure by a degradation process commonly known as irradiation assisted stress corrosion cracking (IASCC). Some of these failures have been reported for components subjected to relatively low or negligible stress levels, e.g., control-blade sheaths and handles and instrument dry tubes of BWRs. Although most failed components can be replaced, some safety-significant structural components, such as the BWR top guide, shroud, and core plate, would be very difficult or impractical to replace. Research during the past six months has focused on (a) fatigue of ferritic steels used in piping, steam generators, and pressure vessels; (b) EAC of cast austenitic SSs; (c) IASCC in high- and commercial-purity (HP and CP) Type 304 SS specimens from control blade absorber tubes and a control-blade sheath used in operating BWRs; and (d) EAC of ferritic steels.

# 2 Fatigue of Ferritic Steels

Plain carbon and low-alloy steels are used extensively in PWR and BWR steam supply systems as piping and pressure vessel materials. The steels of interest in these applications include A106-Gr B and A333-Gr 6 for seamless pipe and A302-Gr B, A508-2, and A533-Gr B plate for pressure vessels. The ASME Code Section III (Division 1, Subsection NB) includes rules for the construction of nuclear power plant Class 1 components. It recognizes fatigue as a possible mode of failure in pressure vessel steels and piping materials. Figure I-90 of Appendix I to Section III specifies the fatigue design curves for the applicable structural materials. The current Code design curves are based

---

[*] USNRC Information Notice No. 88-08, "Thermal Stresses in Piping Connected to Reactor Coolant Systems," June 22, 1988; Supplement 1, June 24, 1988; Supplement 2, August 4, 1988; Supplement 3, April 11, 1989.

[**] USNRC Information Notice No. 88-11, "Pressurizer Surge Line Thermal Stratification," December 20, 1988.

[***] USNRC Information Notice No. 90-29, "Cracking of Cladding in Its Heat-Affected Zone in the Base Metal of a Reactor Vessel Head," April 30, 1990.

[+] USNRC Information Notice No. 90-04, "Cracking of the Upper Shell-to-Transition Cone Girth Welds in Steam Generators," January, 26, 1990.

[++] USNRC Information Notice No. 91-19, "Steam Generator Feedwater Distribution Piping Damage," March 12, 1991.

primarily on strain-controlled fatigue tests of small polished specimens in air at room temperature.[2] To obtain the Code fatigue design curves, best-fit curves to the experimental data were decreased by a factor of 2 on stress or a factor of 20 on cycles, whichever was more conservative at each point. The factors were intended to account for uncertainties in translating the experimental data of laboratory test specimens to actual reactor components. The factor of 20 on cycles is the product of three subfactors: 2.0 for scatter of data (minimum to mean), 2.5 for size effects, and 4.0 for surface finish, atmosphere, etc.[3] "Atmosphere" was intended to reflect the effects of an industrial environment rather than the controlled environment of a laboratory. The effects of the coolant environment are not explicitly addressed in the Code design curves.

Recent fatigue strain vs. life (S/N) data from the U.S.[4-10] and Japan[11-13] illustrate potentially significant effects of LWR environment on the fatigue resistance of carbon and low-alloy steels. In some cases, failures were observed below the ASME Code fatigue design curve. These results raise the issue of whether the fatigue design curves in Section III are appropriate for the purposes intended and whether they adequately account for environmental effects on fatigue behavior. The factors of 2 and 20 applied to the mean-data curve may not be as conservative as originally intended.

The primary sources of U.S. data on fatigue of ferritic steel in LWR environments are the data obtained by General Electric Co. (GE) in a test loop at the Dresden 1 reactor,[4,5] tests performed by GE/Electric Power Research Institute (EPRI),[6] and the work of Terrell.[7,8] Nearly all these data are on carbon steels. The data from Japan have been compiled in the data base JNUFAD* for "Fatigue Strength of Nuclear Plant Components." The results for A508-Cl 3 low-alloy steel and A333-Gr 6 carbon steel have been published by Higuchi and Iida[11] and Iida et al.[12] and for forged A508-Cl 3 and rolled A533-Gr B low-alloy steels by Nagata et al.[13]

Several trends are clear from the available S/N data. The magnitude of the decrease in fatigue life depends on the alloy composition, temperature, and concentration of dissolved oxygen (DO) in the water. At the very low DO levels characteristic of PWRs and BWRs with hydrogen/water chemistry, environmental effects on fatigue life are modest at all temperatures and strain rates. Fatigue life decreases rapidly as DO increases over a rather narrow range of ≈0.1-0.3 ppm, but further increases up to 8 ppm cause only a modest decrease in life. In oxygenated water, fatigue life strongly depends on temperature and strain rate. At a given strain rate, fatigue life increases by a factor of 5 or more as the temperature is decreased from 288 to 200°C. For the same environment and strain range, fatigue lives can be decreased by a factor of ≈50 by reducing the strain rate from 0.1 to 0.0001%/s. Limited data indicate that only the tensile strain rates (strain rate during the tensile half of the strain cycle) are important in environmentally assisted reduction in fatigue life. Based on the existing S/N data, Argonne National Laboratory (ANL) has developed interim fatigue design curves that take into account temperature, DO level in the water, sulfur level in the steel, and strain rate.[14]

---

* Private communication from M. Higuchi, Ishikawajima-Harima Heavy Industries Co., Japan, to M. Prager of the Pressure Vessel Research Council (PVRC), January 1992. The old database "FADAL" has been revised and renamed "JNUFAD."

The S/N data on carbon and low-alloy steels in water, however, are somewhat limited and do not cover the range of loading conditions found in actual reactor operation. For example, virtually all data in LWR water are at relatively high strain ranges. Furthermore, environmental effects on crack initiation have been considered as a possible mechanism for the reduction in fatigue life.[11,12] High-sulfur steels are more susceptible because cracks can initiate at surface micropits that form near manganese sulfide (MnS) inclusions. Effects of crack initiation are important only at low strain ranges, where experimental data are not available. At high strain ranges, fatigue life is dominated by crack propagation.

The data also do not extend over the range of strain rates normally encountered in service; e.g., some transients may have strain rates as low as 0.00001%/s. Extrapolation of available data to such low values would predict a reduction in fatigue life by a factor of >300. The relatively good service experience of carbon steel piping in BWRs, i.e., 288°C water with 0.2 ppm DO, suggests that the effect of strain rate on fatigue life must saturate at some level, although no such saturation has been observed experimentally. The JNUFAD data show that environmental effects on fatigue life are greater for carbon steel than for low-alloy steel.[11] However, most low-alloy steels that have been investigated in JNUFAD are low-sulfur heats (<0.007 wt.%). It is likely that differences between carbon and low-alloy steels are caused by the sulfur content of the steels and that compositional or structural differences have only minor effects on fatigue life.

## 2.1 Technical Progress (O. K. Chopra, W. F. Michaud, and W. J. Shack)

The objectives of this task are to (a) conduct fatigue tests on carbon and low-alloy steels under conditions where information is lacking in the existing S/N data base, (b) establish the effects of material and loading variables on environmentally assisted reduction in fatigue life, and (c) validate and update the proposed interim fatigue design curves. Fatigue tests are being conducted on A106-Gr B carbon steel and A533-Gr B low-alloy steel in water and in air at 288°C. Initial results have been presented earlier.[9,10] For both carbon and low-alloy steels, environmental effects are modest in PWR water at all strain rates. The experimental effort during the present reporting period focused on the effects of strain rate and alloy composition on fatigue life in simulated BWR water. Several fatigue tests were completed on A106-Gr B and A533-Gr B steels at 288°C in water containing ≈0.8 ppm DO to confirm the strong effect of strain rate on fatigue life and to determine whether the strain-rate effect saturates at very low values.

### 2.1.1 Experimental

Low-cycle fatigue tests are being conducted on A106-Gr B carbon steel and A533-Gr B low-alloy steel with an MTS closed-loop electrohydraulics machine. The A533-Gr B material was obtained from the lower head of the Midland reactor vessel, which was scrapped before the plant was completed. The A106-Gr B material was obtained from a 508-mm-diameter schedule 140 pipe fabricated by the Cameron Iron Works, Houston, TX. The chemical compositions of the two materials are given in Table 1, and average room-temperature tensile properties are given in Table 2. Microstructures of the steels are shown in Fig. 1; carbon steel has a pearlitic structure, whereas the low-alloy steel consists of tempered bainite. Smooth cylindrical specimens with 9.5-mm diameter and 19-mm

*Table 1. Chemical composition (wt.%) of ferritic steels used for fatigue tests*

| Material | Source/ Reference[a] | C | P | S | Si | Fe | Cr | Ni | Mn | Mo |
|---|---|---|---|---|---|---|---|---|---|---|
| | | | | | <u>Carbon Steel</u> | | | | | |
| A106-Gr B[b] | ANL | 0.29 | 0.013 | 0.015 | 0.25 | Bal | 0.19 | 0.09 | 0.88 | 0.05 |
| | Supplier | 0.29 | 0.016 | 0.015 | 0.24 | Bal | - | - | 0.93 | - |
| A106-Gr B | Terrell (7) | 0.26 | 0.008 | 0.020 | 0.28 | Bal | 0.015 | 0.002 | 0.92 | 0.003 |
| A333-Gr 6 | Higuchi (11) | 0.20 | 0.020 | 0.015 | 0.31 | Bal | - | - | 0.93 | - |
| | | | | | <u>Low-Alloy Steel</u> | | | | | |
| A533-Gr B[c] | ANL | 0.22 | 0.010 | 0.012 | 0.19 | Bal | 0.18 | 0.51 | 1.30 | 0.48 |
| | Supplier | 0.20 | 0.014 | 0.016 | 0.17 | Bal | 0.19 | 0.50 | 1.28 | 0.47 |
| A533-Gr B | JNUFAD | 0.19 | 0.020 | 0.010 | 0.27 | Bal | 0.13 | 0.60 | 1.45 | 0.52 |

[a] Reference number given within parentheses.

[b] Schedule 140 pipe 508-mm O.D. fabricated by Cameron Iron Works, Heat J-7201. Actual heat treatment not known.

[c] Hot-pressed plate 162 mm thick from Midland reactor lower head. Austenitized at 871-899°C for 5.5 h and brine quenched, then tempered at 649-663°C for 5.5 h and brine quenched. The plate was machined to a final thickness of 127 mm. The I.D. surface was inlaid with 4.8-mm weld cladding and stress relieved at 607°C for 23.8 h.

*Table 2. Average room-temperature tensile properties of ferritic steels*

| Material | Reference[a] | Yield Stress (MPa) | Ultimate Stress (MPa) | Elongation (%) | Reduction in Area (%) |
|---|---|---|---|---|---|
| | | | <u>Carbon Steel</u> | | |
| A106-Gr B | ANL | 301 | 572 | 23.5 | 44.0 |
| A106-Gr B | Terrell (7) | 300 | 523 | 36.6 | 66.3 |
| A333-Gr 6 | Higuchi (11) | 302 | 489 | 41.0 | 80.0 |
| | | | <u>Low-Alloy Steel</u> | | |
| A533-Gr B | ANL | 431 | 602 | 27.8 | 66.6 |
| A533-Gr B | JNUFAD | 488 | 630 | 27.7 | 65.2 |

[a] Reference number given within parentheses.

gage length were used for the fatigue tests (Fig. 2). Specimen gage length was given a 1-μm surface finish in the axial direction to prevent circumferential scratches that might act as sites for crack initiation.

Tests in water were conducted in a small autoclave with an annular volume of 12 mL (Fig. 3). A schematic representation of the system is shown in Fig. 4. The once-through system consists of a 132-L supply tank, Pulsafeeder™ pump, heat exchanger, preheater, and the autoclave. Water is circulated at a rate of ≈10 mL/min and a system pressure of

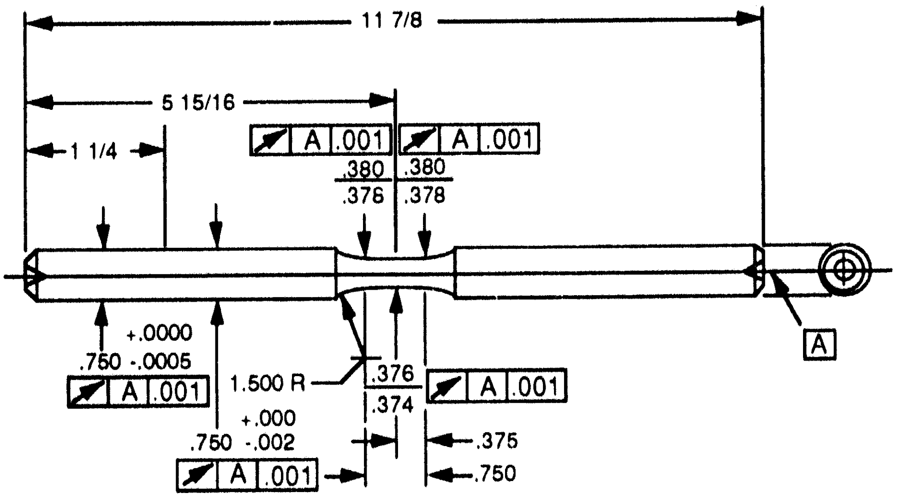

*Figure 1. Configuration of fatigue test specimen (all dimensions in inches)*

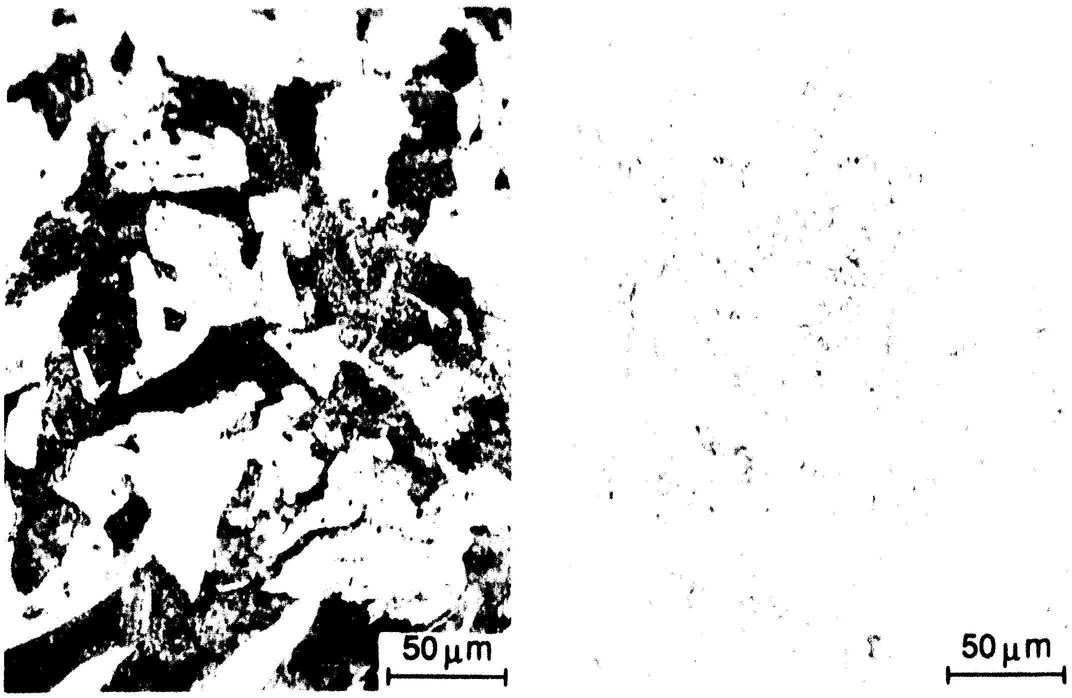

(a)

(b)

*Figure 2. Microstructures of (a) A106-Gr B carbon steel and (b) A533-Gr B low-alloy steel*

9 MPa. The autoclave is constructed of Type 316 SS and contains a titanium liner. The supply tank and most of the low-temperature piping are Type 304 SS; titanium tubing is used in the heat exchanger and for connections to the autoclave and the electrochemical potential (ECP) cell. The ECPs of platinum and an electrode constructed of the same material as the fatigue specimen were monitored during the test against an 0.1 M KCl/AgCl/Ag external reference electrode. An Orbisphere meter and CHEMetrics™ ampules were used to measure the DO concentrations in the supply and effluent water.

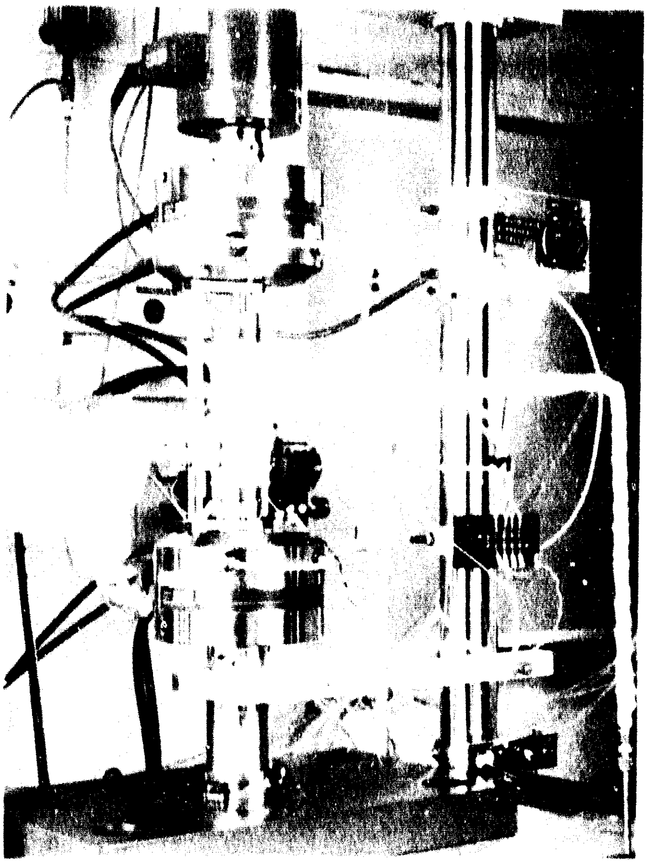

*Figure 3. Autoclave system for fatigue tests in water*

All tests were conducted at 288°C with fully reversed axial loading (i.e., strain ratio R = −1) and a triangular or sawtooth wave form. Unless otherwise mentioned, the strain rate for the triangular wave and fast-loading half of the sawtooth wave was 0.4 %/s. Tests in water were performed under stroke control where the specimen strain was controlled between two locations outside of the autoclave. The fixture and linear-voltage-differential transducer (LVDT) for stroke control can be seen to the left of the autoclave in Fig. 3. Tests in air were performed under strain control with an axial extensometer; specimen strain between the two locations used in the water tests was also recorded. Information from the air tests was used to determine actual strain in the specimen gage length for tests in water.

Simulated BWR water containing ≈0.8 ppm DO was prepared by bubbling nitrogen containing 1–2% oxygen through deionized water in the supply tank. Water samples were taken periodically to measure the pH, resistivity, and DO concentration. After the desired concentration of DO was achieved, the nitrogen/oxygen gas mixture was maintained on the supply tank at a 20-kPa overpressure. Simulated PWR water was formulated by dissolving boric acid and lithium hydroxide in 20 L of deionized water before adding the solution to the supply tank. The DO in deionized water was reduced to <10 ppb by bubbling nitrogen through the water. A vacuum was drawn on the tank cover gas to speed deoxygenation. After the DO was reduced to the desired level, a 20-kPa overpressure of hydrogen was maintained to provide ≈2 ppm dissolved hydrogen in the deoxygenated feedwater.

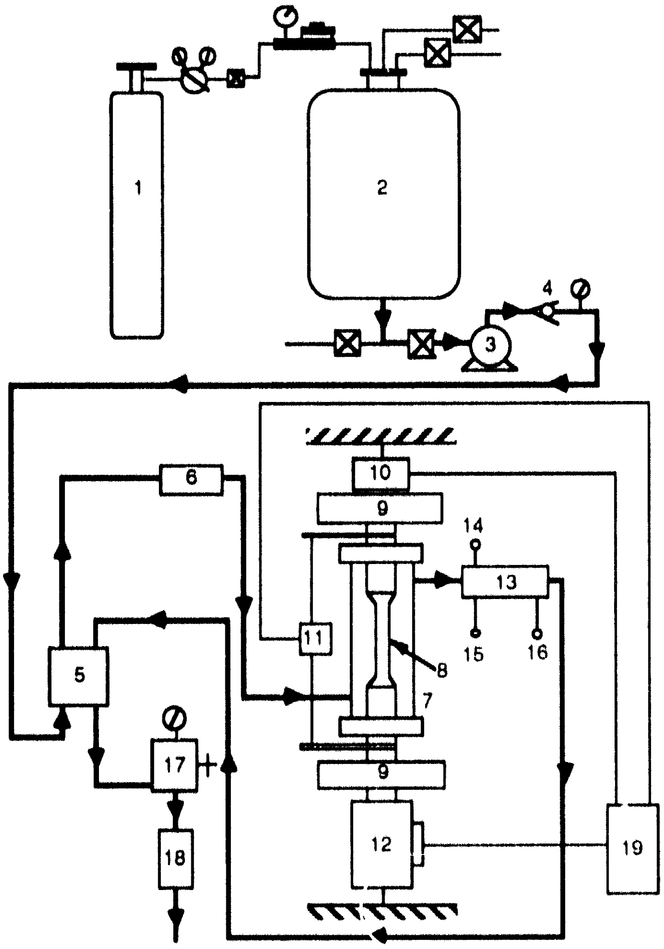

1. Cover gas supply tank
2. Water supply tank
3. Pulsafeeder high-pressure pump
4. Check valve
5. Heat exchanger
6. Preheat exchanger
7. Pipe autoclave
8. Fatigue test specimen
9. MTS hydraulic collet grips
10. MTS load cell
11. Displacement LVDT
12. MTS hydraulic actuator
13. ECP cell
14. Platinum electrode
15. Specimen electrode
16. Reference electrode
17. Mity Mite back-pressure regulator
18. Orbisphere dissolved oxygen meter
19. MTS electrohydraulic controls

*Figure 4. Schematic diagram of autoclave system for fatigue tests in water environment*

### 2.1.2 Results

The fatigue results on A106-Gr B and A533-Br B steels are summarized in Tables 3 and 4, respectively. The fatigue life, $N_{25}$, corresponds to the number of cycles for a 25% decrease in tensile stress amplitude. The total strain range vs. fatigue life curves for the carbon and low-alloy steels in air are shown in Figs. 5 and 6. Results from other investigations[8,11] on similar steels with comparable composition, in particular the sulfur content, and the ASME Section III mean-data curves are also included in the figures.

The results indicate that for both steels, strain rate has no effect on fatigue life in air. The data for A106-Gr B steel are in excellent agreement with results obtained by Terrell[7,8] on A106-Gr B steel, but are lower by a factor of $\approx 5$ than those obtained by Higuchi and Iida[11] on A333-Gr 6 steel. Also, the data for A106-Gr B steel are below the ASME mean-data curve for carbon steel at room temperature at high strain range (by a factor of 3), but are above the ASME mean curve at low strain range. The results for A533-Gr B steel show good agreement with the JNUFAD data on A533-Gr B steel and the ASME mean-data curve for low-alloy steel at room temperature.

*Table 3. Fatigue test results for A106–Gr B steel at 288°C*

| Test Number | Environment | Dissolved Oxygen (ppb) | pH at 25°C | Cond. ($\mu S \cdot cm^{-1}$) | Control[a] | Tensile Rate (%/s) | Comp. Rate (%/s) | Stress Range (MPa) | Strain Range (%) | Life $N_{25}$ (Cycles) |
|---|---|---|---|---|---|---|---|---|---|---|
| 1498 | Air | – | – | – | Strain | 0.4 | 0.4 | 1001.4 | 1.004 | 1,048 |
| 1553 | Air | – | – | – | Strain | 0.4 | 0.4 | 921.1 | 0.757 | 3,253 |
| 1615 | Air | – | – | – | Strain | 0.04 | 0.4 | 959.8 | 0.755 | 3,873 |
| 1609 | Air | – | – | – | Strain | 0.004 | 0.4 | 1026.0 | 0.756 | 3,721 |
| 1543 | Air | – | – | – | Strain | 0.4 | 0.4 | 818.2 | 0.502 | 14,525 |
| 1619 | Air | – | – | – | Strain | 0.4 | 0.4 | 741.7 | 0.401 | 37,142 |
| 1621 | Air | – | – | – | Strain | 0.01 | 0.4 | 787.1 | 0.403 | 38,128 |
| 1550 | Air | – | – | – | Strain | 0.4 | 0.4 | 681.7 | 0.353 | 66,768 |
| 1552 | Air | – | – | – | Strain | 0.4 | 0.4 | 680.6 | 0.352 | 93,322 |
| 1644 | Air | – | – | – | Strain | 0.004 | 0.4 | 702.0 | 0.364 | >95,000 |
| 1546 | Air | – | – | – | Stroke | 0.4 | 0.4 | 975.7 | 0.916 | 1,365 |
| 1612 | Air | – | – | – | Stroke | 0.004 | 0.4 | 1008.2 | 0.779 | 3,424 |
| 1554 | Air | – | – | – | Stroke | 0.4 | 0.4 | 896.8 | 0.730 | 3,753 |
| 1548 | Air | – | – | – | Stroke | 0.4 | 0.4 | 831.9 | 0.545 | 10,632 |
| 1555 | Air | – | – | – | Stroke | 0.4 | 0.4 | 676.3 | 0.343 | 98,456 |
| 1547 | PWR[b] | 8 | 6.7 | 23.3 | Stroke | 0.4 | 0.4 | 1010.9 | 0.987 | 692 |
| 1564 | PWR[b] | 12 | 6.6 | 21.7 | Stroke | 0.4 | 0.4 | 942.0 | 0.769 | 1,525 |
| 1549 | PWR[b] | 8 | 6.7 | 25.6 | Stroke | 0.4 | 0.4 | 827.0 | 0.533 | 9,396 |
| 1560 | PWR[b] | 12 | 6.6 | 23.7 | Stroke | 0.4 | 0.4 | 701.3 | 0.363 | 35,100 |
| 1556 | PWR[b] | 8 | 6.6 | 22.7 | Stroke | 0.4 | 0.4 | 710.9 | 0.360 | 38,632 |
| 1632 | BWR | 800 | 5.8 | 0.11 | Stroke | 0.4 | 0.4 | 913.3 | 0.740 | 2,077 |
| 1614 | BWR | 400 | 5.9 | 0.11 | Stroke | 0.004 | 0.4 | 930.4 | 0.786 | 303 |
| 1623 | BWR | 800 | 5.9 | 0.08 | Stroke | 0.004 | 0.004 | 943.8 | 0.792 | 338 |
| 1616 | BWR | 800 | 5.8 | 0.08 | Stroke | 0.0004 | 0.4 | 912.8 | 0.799 | 153 |
| 1620 | BWR | 900 | 5.9 | 0.11 | Stroke | 0.00004 | 0.004 | 943.1 | 0.794 | 161 |
| 1634 | BWR | 800 | 5.8 | 0.16 | Stroke | 0.4 | 0.4 | 733.2 | 0.400 | 19,318 |
| 1624 | BWR | 800 | 5.9 | 0.10 | Stroke | 0.004 | 0.4 | 775.7 | 0.456 | 2,276 |
| 1639 | BWR | 800 | 5.9 | 0.09 | Stroke | 0.004 | 0.4 | 751.6 | 0.418 | 2951 |

[a] Values for stroke–control tests are approximate. Actual strain rates are ±5% of the listed value.

[b] Contains 2 ppm lithium and 1000 ppm boron.

The total strain range vs. fatigue life plots for A106–Gr B and A533–Gr B steels in simulated PWR water containing <10 ppb DO, 1000 ppm boron, and 2 ppm lithium are shown in Figs. 7 and 8, respectively. The results indicate a marginal effect of PWR water on fatigue life at high strain ranges. For both steels, fatigue lives in PWR water are up to a factor of 2 lower than those in air at a strain range >0.5%. Fatigue lives in water and air environments are comparable at a strain range <0.5%. Limited data on A533–Gr B steel indicate that a decrease in the strain rate by two orders of magnitude does not cause an additional decrease in fatigue life. The results for A106–Gr B steel are consistent with the data obtained by Terrell[8] in simulated PWR water where no noticeable effect of strain rate or environment on fatigue life was observed (Fig. 7). The results are also consistent with the data of Iida et al.[12] and Prater and Coffin,[15,16] in which the effects of environment were minimal at DO levels of <100–200 ppb.

The effect of oxygenated water (0.8 ppm DO) on fatigue life of A106–Gr B and A533–Gr B steels is shown in Figs. 9 and 10, respectively. The results indicate that environmental effects depend strongly on strain rate and that only strain rate during the tensile half of a strain cycle is important. The steels show identical behavior; fatigue life

*Table 4. Fatigue test results for A533-Gr B steel at 288°C*

| Test Number | Environment | Dissolved Oxygen (ppb) | pH at 25°C | Cond. (μS·cm⁻¹) | Control[a] | Tensile Rate[a] (%/s) | Comp. Rate[a] (%/s) | Stress Range (MPa) | Strain Range (%) | Life $N_{25}$ (Cycles) |
|---|---|---|---|---|---|---|---|---|---|---|
| 1508 | Air | – | – | – | Strain | 0.4 | 0.4 | 910.9 | 1.002 | 3,305 |
| 1515 | Air | – | – | – | Strain | 0.4 | 0.4 | 866.1 | 0.752 | 6,792 |
| 1625 | Air | – | – | – | Strain | 0.004 | 0.4 | 887.7 | 0.757 | 4,592 |
| 1505 | Air | – | – | – | Strain | 0.4 | 0.4 | 767.6 | 0.501 | 31,200 |
| 1576 | Air | – | – | – | Strain | 0.004 | 0.4 | 805.8 | 0.503 | 28,129 |
| 1590 | Air | - | - | - | Strain | 0.4 | 0.004 | 821.1 | 0.503 | 24,471 |
| 1640 | Air | – | – | – | Strain | 0.4 | 0.4 | 710.9 | 0.402 | 65,880 |
| 1517 | Air | – | – | – | Strain | 0.4 | 0.4 | 692.5 | 0.353 | 2,053,295 |
| 1521 | Air | – | – | – | Stroke | 0.4 | 0.4 | 889.4 | 0.910 | 3,219 |
| 1523 | Air | - | - | - | Stroke | 0.4 | 0.4 | 898.6 | 0.917 | 2,206 |
| 1522 | Air | – | – | – | Stroke | 0.4 | 0.4 | 905.4 | 0.899 | 3,419 |
| 1524 | Air | – | – | – | Stroke | 0.4 | 0.4 | 892.3 | 0.950 | 3,714 |
| 1525 | Air | – | – | – | Stroke | 0.4 | 0.4 | 743.6 | 0.452 | 65,758 |
| 1538 | Air | – | – | – | Stroke | 0.4 | 0.4 | 708.0 | 0.387 | >1,000,000 |
| 1526 | DI[b] | 16 | – | – | Stroke | 0.4 | 0.4 | 876.4 | 0.873 | 3,332 |
| 1527 | DI[b] | 17 | 6.0 | – | Stroke | 0.4 | 0.4 | 752.8 | 0.493 | 10,292 |
| 1528 | DI[b] | 5 | 5.8 | – | Stroke | 0.4 | 0.4 | 744.1 | 0.488 | 25,815 |
| 1530 | PWR[c] | 3 | 6.9 | 41.7 | Stroke | 0.4 | 0.4 | 885.5 | 0.894 | 1,355 |
| 1545 | PWR[c] | 8 | 6.9 | 22.7 | Stroke | 0.4 | 0.4 | 889.7 | 0.886 | 3,273 |
| 1533 | PWR[c] | 4 | 6.9 | 45.5 | Stroke | 0.004 | 0.4 | 916.0 | 0.774 | 3,416 |
| 1529 | PWR[c] | 3 | 6.9 | 45.5 | Stroke | 0.4 | 0.4 | 743.4 | 0.484 | 31,676 |
| 1588 | PWR[c] | 6 | 6.5 | 23.3 | Stroke | 0.004 | 0.4 | 828.7 | 0.514 | 15,321 |
| 1605 | PWR[c] | 9 | 6.5 | 23.8 | Stroke | 0.4 | 0.004 | 785.2 | 0.460 | >57,443 |
| 1539 | PWR[c] | 6 | 6.8 | 38.5 | Stroke | 0.4 | 0.4 | 694.8 | 0.373 | 136,570 |
| 1542 | PWR[c] | 6 | 6.6 | 27.0 | Stroke | 0.4 | 0.4 | 631.8 | 0.354 | >1,154,892 |
| 1645 | BWR | 800 | 6.1 | 0.07 | Stroke | 0.4 | 0.4 | 831.1 | 0.721 | 2,736 |
| 1626 | BWR | 900 | 5.9 | 0.13 | Stroke | 0.004 | 0.4 | 910.1 | 0.788 | 247 |
| 1627 | BWR | 800 | 5.9 | 0.10 | Stroke | 0.004 | 0.4 | 826.8 | 0.534 | 769 |
| 1641 | BWR | 800 | 5.9 | 0.09 | Stroke | 0.4 | 0.4 | 693.0 | 0.374 | 17,367 |
| 1647 | BWR | 800 | 6.1 | 0.09 | Stroke | 0.4 | 0.4 | 688.0 | 0.363 | 26,165 |

[a] Values for stroke-control tests are approximate. Actual strain rates are ±5% of the listed value.

[b] Deionized water.

[c] Contains 2 ppm lithium and 1000 ppm boron.

decreases rapidly with a decrease in strain rate. Compared with tests in air, fatigue life in oxygenated water is lower by a factors of 2 and 10 at strain rates of 0.4 and 0.004 %/s, respectively. Fatigue tests were conducted on A106-Gr B steel, at a total strain range of ≈0.75% with a sawtooth wave form and tensile strain rates between 0.4 and 0.00004 %/s, to establish the effect of strain rate on fatigue life. Relative fatigue life, i.e., ratio of fatigue life in water to that in air, is plotted as a function of strain rate in Fig. 11. The results indicate that the effect of strain rate saturates at ≈0.0004 %/s; fatigue life in water is lower by a factor of 20 lower than in air. The results also indicate that only the slow tensile-strain cycle is responsible for environmentally assisted reduction in fatigue life. Two fatigue tests on A106-Gr B steel at a strain range of ≈0.75, one with a sawtooth wave form (i.e., 0.004 and 0.4%/s strain rates, respectively, during the tensile and compressive half of the strain cycle) and the other with a triangle wave form (i.e., 0.004 %/s constant strain rate), show identical fatigue lives (Fig. 9).

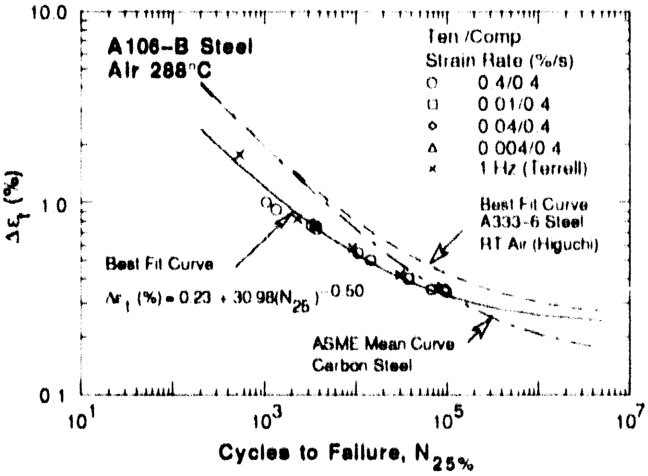

*Figure 5.*
*Total strain range vs. fatigue life data for A106-Gr B steel in air*

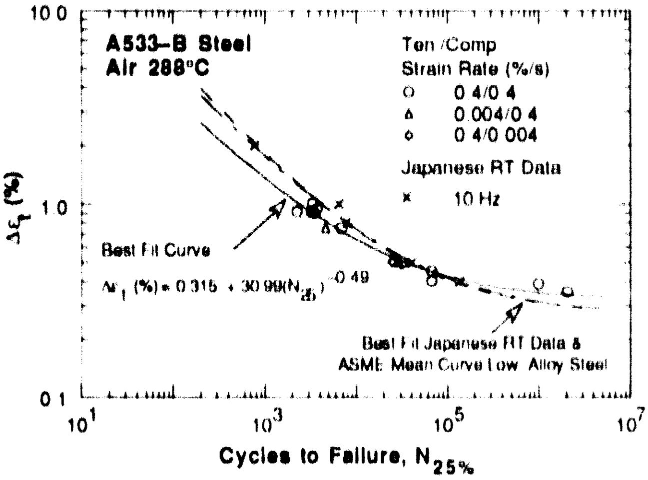

*Figure 6.*
*Total strain range vs. fatigue life data for A533-Gr B steel in air*

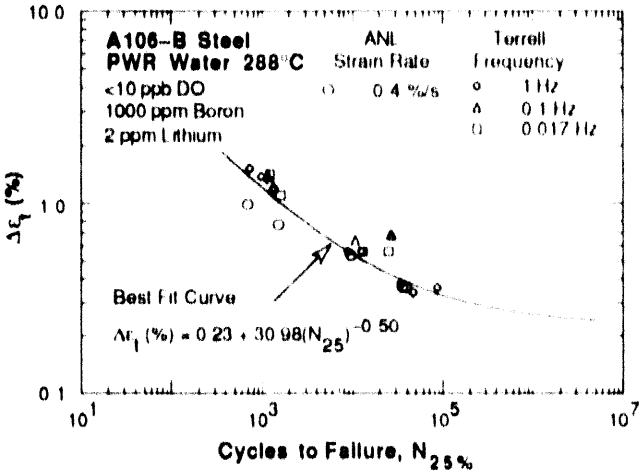

*Figure 7.*
*Total strain range vs. fatigue life data for A106-Gr B steel in PWR water at 288°C*

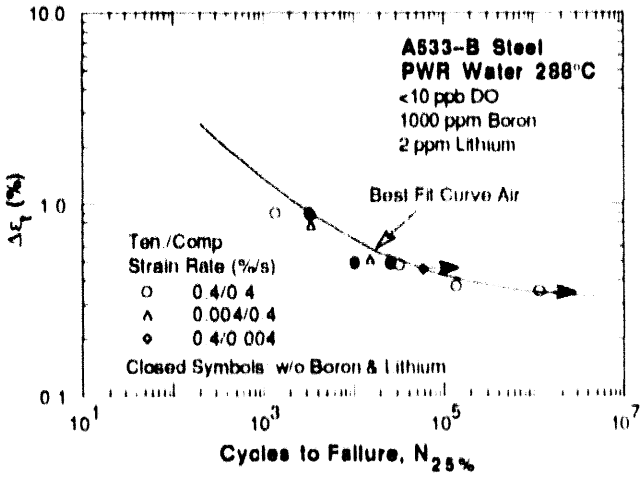

*Figure 8.*
*Total strain range vs. fatigue life data for A533 Gr B steel in PWR water at 288°C*

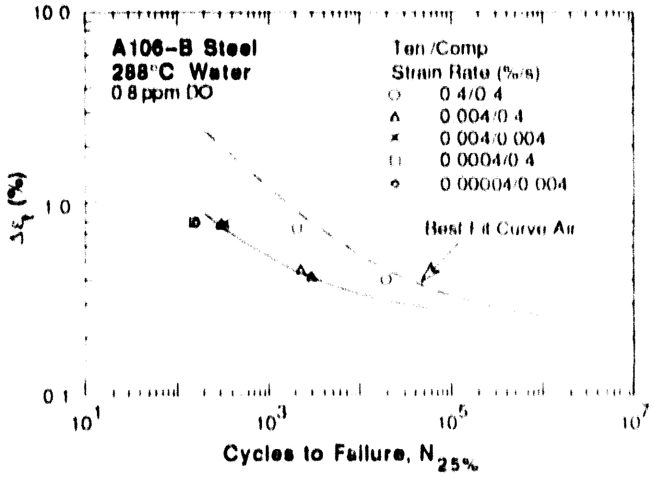

*Figure 9.*
*Total strain range vs. fatigue life data for A106 Gr B steel in high oxygen water at 288°C*

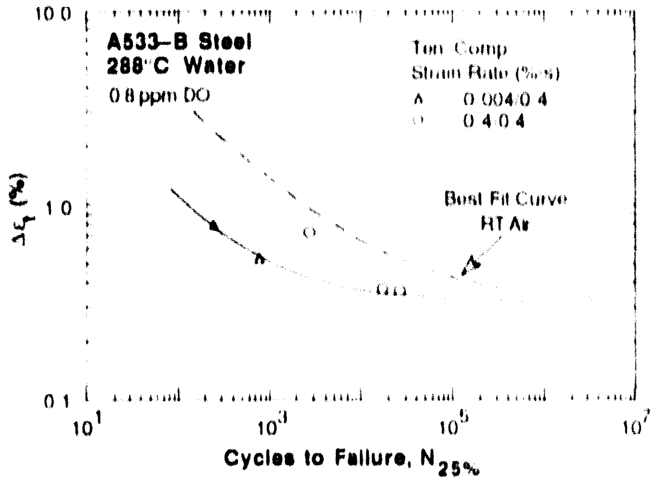

*Figure 10.*
*Total strain range vs. fatigue life data for A533 Gr B steel in high oxygen water at 288°C*

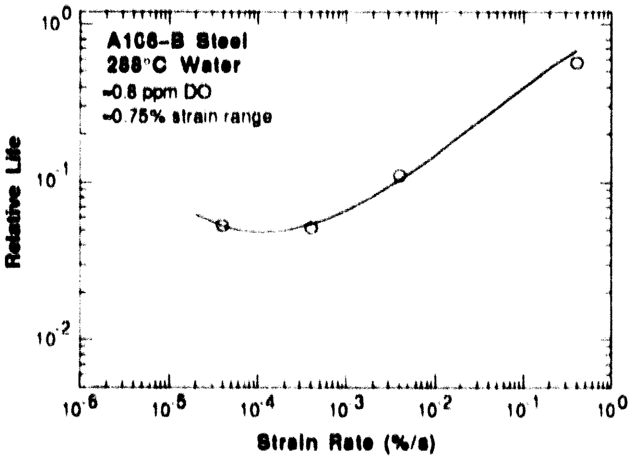

*Figure 11.*
*Effect of strain rate on fatigue life of A106-Gr B steel in high-oxygen water at 288°C. Relative life is the ratio of fatigue life in water to that in air.*

Plots of cyclic stress range vs. fatigue cycles for A106-Gr B and A533-Gr B steels tested in air at 288°C and a total strain range of ~0.75% are shown in Figs. 12 and 13, respectively. The cyclic strain-hardening behavior of the steels is consistent with their microstructure. The A106-Gr B steel, with a pearlitic structure and low yield stress, exhibits rapid hardening during the initial 100 cycles of fatigue life. The extent of hardening increases with applied strain range. The A106-Gr B carbon steel also shows significant dynamic strain aging, e.g., cyclic stress increases throughout the test. Fatigue strength of the material increases with decreasing strain rate without affecting its fatigue life significantly (Fig. 12). In contrast, the A533-Gr B low-alloy steel consists of a bainitic structure, has a relatively high yield stress, and shows little or no initial hardening and dynamic strain aging (Fig. 13). At low strain ranges, the A533-Gr B steel shows cyclic softening during the initial 100 cycles of fatigue life (Fig. 14).

The cyclic stress vs. strain curves for A106-Gr B and A533-Gr B steels at 288°C are shown in Figs. 15 and 16, respectively; cyclic stress corresponds to the value at half life. The results for A106-Gr B steel show excellent agreement with the data obtained by Terrell.[8] The total strain range $\Delta\varepsilon_t$ (%) can be expressed in terms of the cyclic stress range (MPa) with the equation obtained by Terrell at 288°C:

$$\Delta\varepsilon_t = \frac{\Delta\sigma}{1907.8} + \left(\frac{\Delta\sigma}{1010.43}\right)^{11.546}. \tag{1}$$

The best-fit stress vs. strain curve for A533-Gr B steel is represented by

$$\Delta\varepsilon_t = \frac{\Delta\sigma}{1965.0} + \left(\frac{\Delta\sigma}{956.0}\right)^{11.1}. \tag{2}$$

For both steels, an aqueous environment has little or no effect on the cyclic stress-strain behavior. The effect of strain rate on the cyclic stress-strain is quite pronounced in A106-Gr B carbon steel because of dynamic strain aging of the material, whereas strain rate has a modest effect on the cyclic stress-strain curve for A533-Gr B low-alloy steel.

In general, the surfaces of A106-Gr B and A533-Gr B specimens tested in simulated PWR water developed a grey/black corrosion scale. In addition, the specimens tested in water containing 0.8 ppm DO showed patches of a loose brown/red deposit. Micrographs

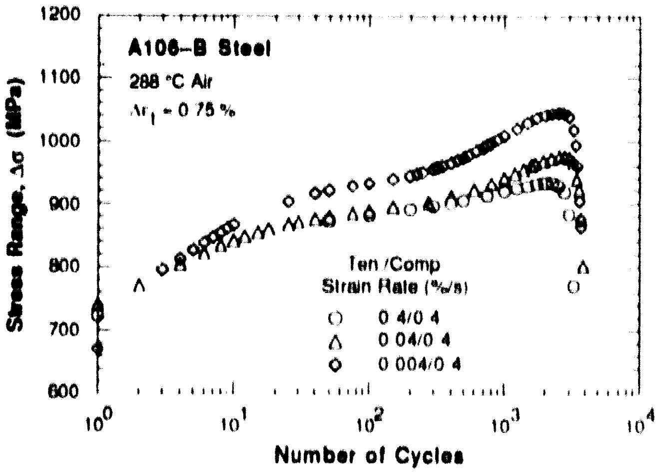

*Figure 12.*
*Effect of strain rate on cyclic strain-hardening behavior of A106-Gr B steel in air at 288°C*

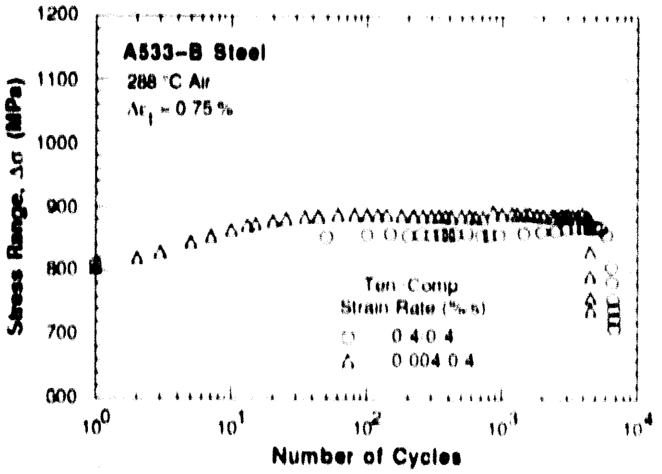

*Figure 13.*
*Effect of strain rate on cyclic strain-hardening behavior of A533-Gr B steel in air at 288°C*

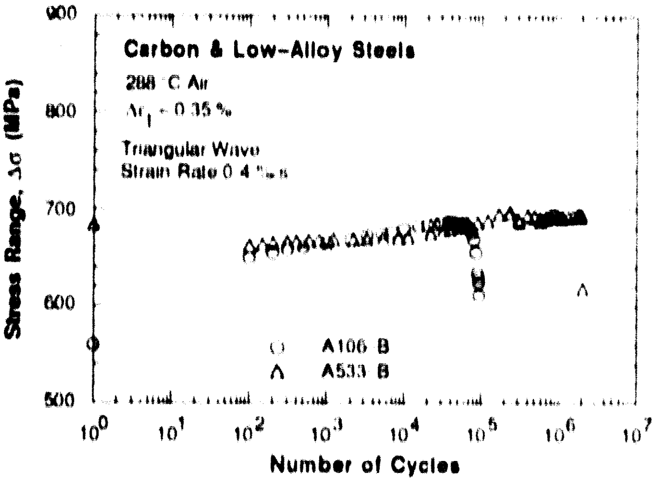

*Figure 14.*
*Cyclic strain-hardening behavior of A106-Gr B and A533-Gr B steels at 0.35% total strain range and 0.4 %/s strain rate in air*

of the gage surface of the steels tested in air and simulated PWR and BWR water are shown in Fig. 17. X-ray diffraction analysis of the specimen surfaces indicated that for both steels, the corrosion scale is primarily magnetite ($Fe_3O_4$) in simulated PWR water but also contains some hematite ($Fe_2O_3$) after exposure to deionized water containing ≈0.8 ppm DO.

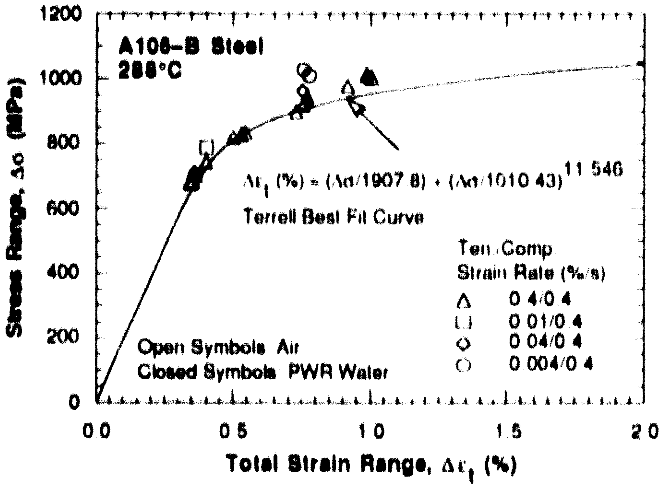

*Figure 15.*
*Cyclic stress–strain curve for A106–Gr B steel at 288°C in air and water environments*

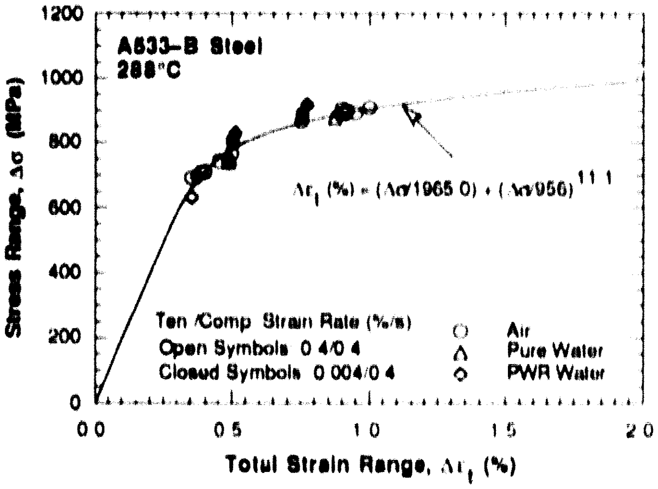

*Figure 16.*
*Cyclic stress–strain curve for A533–Gr B steel at 288°C in air and water environments*

All specimens tested in water showed surface micropitting. Most likely, these surface pits formed by selective dissolution of MnS inclusions. Typical examples of micropits on A533–Gr B low-alloy steel in simulated PWR water and deionized water containing ≈0.8 ppm DO are shown in Fig. 18. These pits can act as sites for crack initiation; they are often associated with cracks. A detailed examination of gage length surfaces of the fatigue test specimens is in progress to establish the effect of the aqueous environments on crack initiation.

### 2.1.3 Discussion

Fatigue data in oxygenated water reveal significant reductions in fatigue life and a strong dependence on strain rate. However, there is little difference in environmental degradation of fatigue life between A106–Gr B carbon steel and A533–Gr B low-alloy steel that contain comparable sulfur levels. Although the cyclic stress–strain and cyclic hardening behavior is distinctly different, the reduction in fatigue life of the two steels is comparable or somewhat greater for the low-alloy steel (Figs. 9 and 10). The carbon steel also exhibits pronounced dynamic strain aging, whereas strain aging effects are modest in the low-alloy steel.

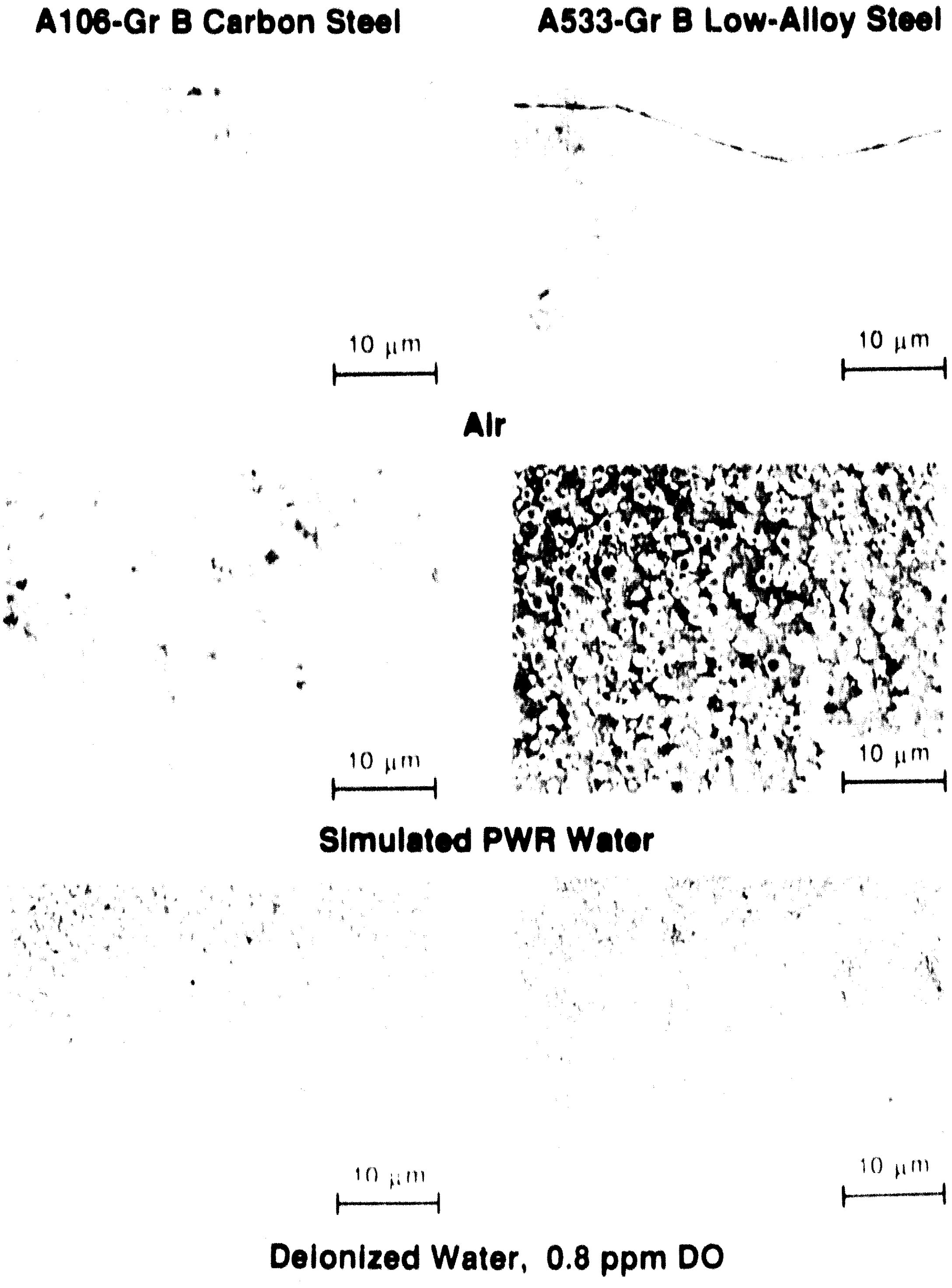

*Figure 17. SEM micrographs of gage surface of A106 Gr B and A533 Gr B steels tested in different environments at 288°C*

The results also indicate that in oxygenated water, fatigue life depends not only on strain rate but also on DO concentration. The relative fatigue lives of ANL and JNUFAD heats of carbon and low alloy steels with comparable sulfur contents, are plotted as a

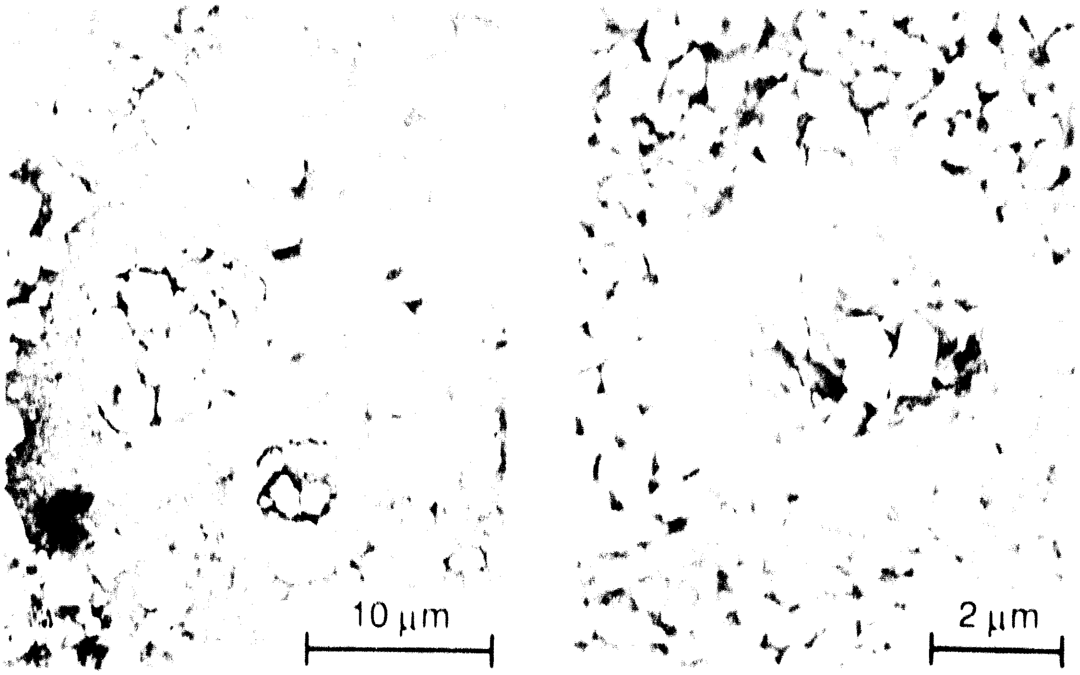

*Figure 18. SEM micrographs of micropits on gage surface of A106 Gr B and A533 Gr B steels tested in different environments at 288°C*

function of strain rate in Figs. 19 and 20. Environmental effects increase with increasing levels of DO. For both steels, the maximum reduction in fatigue life is a factor of 2 at <0.01 ppm DO and a factor of 50 or more at 8 ppm DO. Fatigue lives in water at intermediate values of DO are between these limits. The results also indicate that the effect of strain rate on fatigue life saturates at some low value of strain rate. The existing data are inadequate to determine whether the saturation value of strain rate varies with DO and/or alloy composition. The effect of strain rate saturates at ≈0.0004 %/s for A106 Gr B carbon steel in water containing ≈0.8 ppm DO. Additional fatigue tests are in progress to establish the effects of DO on the reduction in fatigue life and the saturation value of the strain rate.

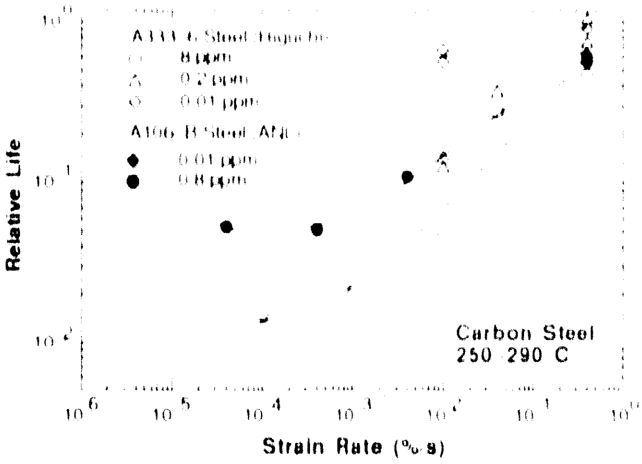

*Figure 19. Relative fatigue life of A106 Gr B carbon steel at different levels of dissolved oxygen and strain rates*

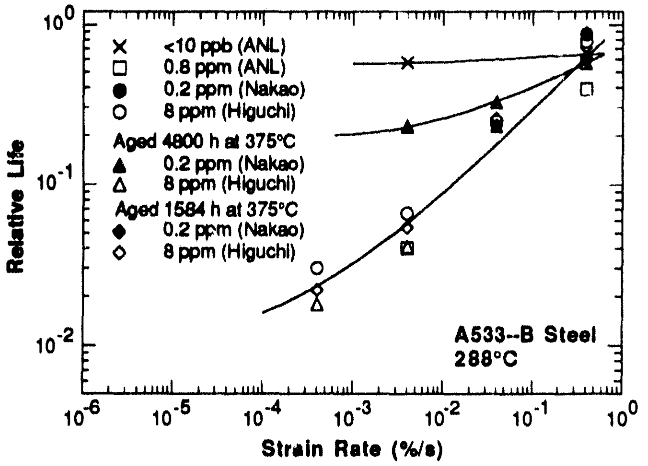

*Figure 20.*
*Relative fatigue life of A533-Gr B low-alloy steel at different levels of dissolved oxygen and strain rates*

## 3 Environmentally Assisted Cracking of Cast SSs in Simulated BWR Water

Cast-duplex SSs are used extensively in the nuclear industry in pump casings, valve bodies, piping, and other components in coolant systems of LWRs. The steels correspond to ASTM Specification A-351 grades CF-3, CF-3A, CF-8, CF-8A, and CF-8M, where the compositions of CF-3A and CF-8A fall within the composition limits of CF-3 and CF-8, but are further restricted to obtain ferrite/austenite ratios that result in higher ultimate and yield strengths. The molybdenum-free CF-3 and CF-8 grades contain low- and high-carbon concentrations (<0.03 and <0.08 wt.%, respectively) and are similar in composition to wrought Types 304L and 304 SS. The Mo-containing CF-3M and CF-8M grades with low- and high-C content are similar to Types 316L and 316 SS, respectively. After many years of service at reactor operating temperatures, these steels can undergo thermal aging embrittlement that is caused by precipitation and growth of a Cr-rich $\alpha'$ phase, an Ni- and Si-rich G phase, $M_{23}C_6$, $\gamma$ (austenite) in the ferrite, and additional precipitation and/or growth of existing carbides at the ferrite/austenite phase boundaries.[17-26] These compositional changes increase the tensile strength and decrease the impact energy and fracture toughness of the steels.[26-37] In general, the low-C CF-3 grade is most resistant and the Mo-bearing high-C CF-8M grade is least resistant to thermal embrittlement.[28,31]

An inspection of the drywell of a BWR to determine the cause of an increase in unidentified leakage revealed a through-wall crack in the manual gate valve in the condensate return line of the emergency condenser system.[*] Subsequently, the internal components of other valves in the emergency condenser system were removed and inspected by visual, radiographic, and ultrasonic tests. Inspections of the inner surface of the valves revealed cracks near drain holes in the valve bodies, which were made from CF-8M SS. Some of the cracks were within 0.15–0.35 in. of passing through the 1.25-in. wall thickness (≈70–90% through wall). A metallographic examination of a boat specimen revealed that the material contained ≈15% delta ferrite and that the crack propagated transgranularly with little secondary cracking, which is characteristic of a fatigue crack.

---

[*] NRC Information Notice 92-50: Cracking of Valves in the Condensate Return Lines of a BWR Emergency Condenser System, July 2, 1992.

The purpose of the present work is to (a) determine whether local compositional changes and concomitant increases in strength of the materials caused by thermal aging can influence EAC under cyclic loading in high-temperature water, and (b) establish whether CGR curves for wrought SS in high-temperature oxygenated water are applicable to cast grades of the steel in the as-received and thermally aged conditions.

## 3.1 Technical Progress (W. E. Ruther, O. K. Chopra, and T. F. Kassner)

During this reporting period, fracture-mechanics CGR tests were completed on three additional 1TCT specimens of cast SS, namely, as-received CF-8 (Heat 68, No. 681-08) and specimens of CF-8 (Heat 68, No. 682-05) and CF-8M (Heat 75, No. 752-04) aged for 30,000 h at 350°C. Results obtained on as-received CF-8M (Heat 75) and specimens of CF-8M (Heat 75) and CF-8 (Heat 68) steel aged for 10,000 h at 400°C were presented in the previous report.[38] As in the case of the previous specimens, the aging condition was sufficient for both heats of steel to reach a "saturation" Charpy-impact energy $Cv_{sat}$, i.e., a minimum value that would be achieved by the materials after very-long-term aging. The actual value of the saturation impact energy for a specific cast SS is independent of aging temperature but depends strongly on the composition of the steel. It is lower for the Mo-bearing CF-3M and CF-8M steels than for the Mo-free CF-3 and CF-8 steels, and decreases with an increase in ferrite content or the C or N concentration in the steels. The room-temperature $Cv_{sat}$ values for cast SSs in thermal aging embrittlement studies conducted at ANL[35] ranged from ≈30 to 162 $J \cdot cm^{-2}$. The room-temperature impact energy values for Heats No. 75 (CF-8M) and 68 (CF-8) aged for 30,000 h at 350°C were 30 and 65 $J \cdot cm^{-2}$, respectively, which are indicative of materials with low fracture toughness after thermal aging. The chemical composition and ferrite content of these steels, and of CF-3 and -3M grades tested previously,[39,40] are given in Table 5.

*Table 5. Chemical composition and ferrite content of cast SSs for corrosion fatigue tests in simulated BWR water*

| Material | Heat | Composition (wt.%) | | | | | | | | | Ferrite (%) | |
|---|---|---|---|---|---|---|---|---|---|---|---|---|
| | No. | Cr | Mo | Ni | Mn | Si | C | N | P | S | Calc. | Meas. |
| CF-8 | 68 | 20.64 | 0.31 | 8.08 | 0.64 | 1.07 | 0.063 | 0.062 | 0.021 | 0.014 | 14.9 | 23.4 |
| CF-8M | 75 | 20.86 | 2.58 | 9.12 | 0.53 | 0.67 | 0.065 | 0.052 | 0.022 | 0.012 | 24.8 | 27.8 |
| CF-3 | P2 | 20.20 | 0.16 | 9.38 | 0.74 | 0.94 | 0.019 | 0.062 | 0.019 | 0.006 | 12.5 | 15.6 |
| CF-3M | F5524 | 19.38 | 2.38 | 11.80 | 0.96 | 1.35 | 0.018 | 0.099 | 0.015 | 0.005 | 5.9 | 5.0 |

CGRs of the as-received CF-8 and aged (30,000 h at 350°C) CF-8 and CF-8M specimens are shown in Table 6. Four tests were conducted in 289°C high-purity (HP) water containing 4–5 ppm DO at a frequency of 0.08 Hz, and stress intensities $K_{max}$ of 30 to 35 $MPa \cdot m^{1/2}$ where the load ratio, R, was varied from 0.3 to 0.9. The oxygen level was then reduced by a factor of 10 (to ≈0.4-0.5 ppm) and several of the tests were repeated. After Test 7, the system was shut down to remove the aged CF-8M specimen that had reached the maximum permissible crack length and the experiment is being continued to investigate the effects of DO concentration on the CGRs of the remaining CF-8 specimens.

*Table 6. Crack growth results for CF–8M and CF–8 Cast SS 1T–compact–tension specimens[a] under cyclic loading[b] in 289°C water*

| | | | | Potentials | | Load | | Rise | CF–8M (No. 752–04) Aged (30,000 h @ 350°C) | | CF–8 (No. 681–08) As–received | | CF–8 (No. 682–05) Aged (30,000 h @ 350°C) | |
|---|---|---|---|---|---|---|---|---|---|---|---|---|---|---|
| Test No. | Time, h | Cond., $\mu S \cdot cm^{-1}$ | $O_2$,[c] ppm | 304 SS, mV(SHE) | Pt, mV(SHE) | Ratio | Freq., $10^{-2}$ Hz | Time, s | $K_{max}$[d], $MPa \cdot m^{1/2}$ | Rate, $10^{-10}$ $m \cdot s^{-1}$ | $K_{max}$[d], $MPa \cdot m^{1/2}$ | Rate, $10^{-10}$ $m \cdot s^{-1}$ | $K_{max}$[d], $MPa \cdot m^{1/2}$ | Rate, $10^{-10}$ $m \cdot s^{-1}$ |
| 1 | 374<br>398 | 0.07 | 4.4 | 256 | 280 | 0.80 | 7.7 | 12 | 31.8 | 58.0 | 30.2 | 16.9 | 30.9 | 31.9 |
| 2 | 398<br>526 | 0.08 | 4.3 | 237 | 243 | 0.90 | 7.7 | 12 | 33.1 | 16.2 | 30.5 | 3.9 | 31.3 | 5.4 |
| 3 | 526<br>565 | 0.07 | 4.2 | 247 | 301 | 0.70 | 7.7 | 12 | 34.9 | 122.0 | 30.9 | 39.2 | 32.1 | 53.7 |
| 4 | 565<br>719 | 0.07 | 4.5 | 252 | 337 | 0.30 | 7.7 | 12 | 38.2 | 349.0 | 32.0 | 170.0 | 33.0 | 157.0 |
| 5 | 719<br>1345 | 0.11 | 0.43 | 205 | 218 | 0.90 | 7.7 | 12 | 40.6 | 15.9 | 32.4 | 2.9 | 33.6 | 4.2 |
| 6 | 1345<br>1410 | 0.07 | 0.60 | 214 | 223 | 0.70 | 7.7 | 12 | 43.8 | 110.0 | 33.1 | 32.8 | 34.4 | 32.4 |
| 7 | 1410<br>1559 | 0.11 | 0.50 | 205 | 211 | 0.30 | 7.7 | 12 | 52.5 | 666.0 | 34.4 | 157.0 | 35.8 | 191.0 |

[a] Heat No. 75 for CF–8M containing 27.8% ferrite (Specimen No. 752–04) and No. 68 for CF–8 containing 23.4% ferrite (Specimens No. 681–08 and 682–05).

[b] Positive sawtooth wave form was used.

[c] Effluent dissolved-oxygen concentrations.

[d] Stress intensity, $K_{max}$, values at the end of the time period.

Figure 21 shows the dependence of the CGRs of as-received and aged CF-8M and CF-8 specimens on DO concentration in HP water from these and previous tests[38] at R values of 0.90–0.95. At DO concentrations >1 ppm, the CGRs of thermally aged CF-8M are higher by one order of magnitude than for the steel in the as-received condition. Thermal aging has a smaller effect on the CGRs of CF-8 SS under these conditions.

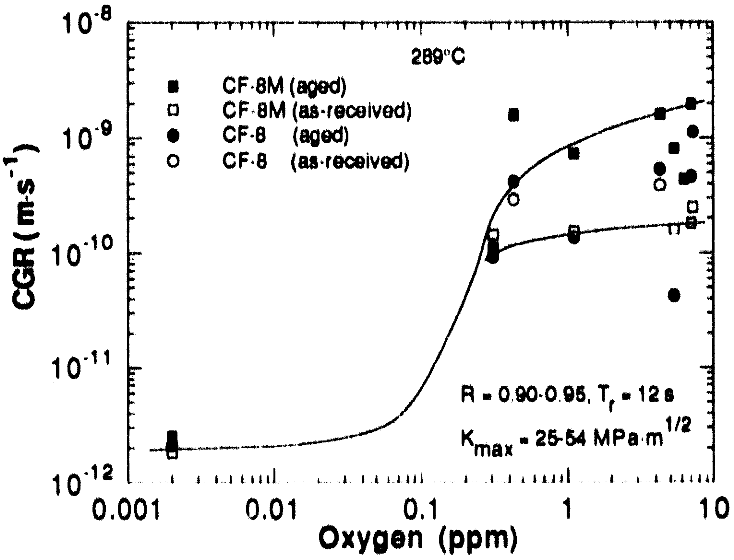

*Figure 21. Crack growth rates of as-received and thermally aged CF-8M and CF-8 grades of cast SS under high-R loading in HP water at 289°C*

The experimental results in Table 7 for these specimens and for as-received CF-3 and CF-3M specimens reported previously[39,40] were compared with predicted CGRs for wrought SSs in air and in water under the various loading conditions (Fig. 22). The lines denoted as $a_{super}$8.0 and $a_{super}$0.2 in Fig. 22 represent predictions from interim correlations developed at Argonne for 289°C water that contains ≈8 and ≈0.2 ppm DO.[41] The predictions of the present correlation for wrought SS in air in Section XI of the ASME code are represented by the diagonal straight lines. Clearly, the air curve is frequently nonconservative. The experimental CGRs for CF-8, -8M, and -3M specimens lie above the air line (solid curve), but for the most part are bounded by CGRs from the modified correlations for wrought SSs in water at 289°C. The CGRs of the CF-3M and CF-8M specimens (with carbon content of 0.018 and 0.065 wt.% and ferrite content of ≈5 and 27.8%, respectively) show the largest environmental enhancement in both the as-received and aged conditions.

*Table 7. Summary of crack growth results for cast SS specimens[a] at different load ratio[b] and stress intensity values in 289°C water*

| Water Chemistry | | | Potentials | | Load | | Rise | CGR Data | | | ANL |
|---|---|---|---|---|---|---|---|---|---|---|---|
| Cond., $\mu S \cdot cm^{-1}$ | $O_2$, ppm | $SO_4^{2-}$, ppb | 304 SS, mV(SHE) | Pt, mV(SHE) | Ratio | Freq., $10^{-2}$ Hz | Time, s | $K_{max}$[c], $MPa \cdot m^{1/2}$ | ΔK,[d] | Rate, $10^{-10}$ $m \cdot s^{-1}$ | Report No. |
| As-received CF-3M Specimen (Heat No. F5524) Containing 5.0% Ferrite | | | | | | | | | | | |
| 0.90 | 0.2 | 100 | 136 | 120 | 0.95 | 7.7 | 12 | 22.6 | 1.13 | 1.90 | 90/4 |
| 0.90 | 0.2 | 100 | 106 | 66 | 0.25[e] | 10.0 | 5 | 20.7 | 15.50 | 35.0 | 90/4 |
| 0.90 | 0.2 | 100 | 81 | 41 | 0.95 | 7.7 | 12 | 24.0 | 1.20 | 2.50 | 90/4 |
| 1.10 | 0.2 | 100 | 134 | 95 | 1.00 | 0 | ∞ | 24.1 | 0 | 0.32 | 90/4 |
| As-received CF-3 Specimen (Heat No. P2) Containing 15.6% Ferrite | | | | | | | | | | | |
| 0.93 | 0.2 | 100 | 150 | 208 | 0.50 | 7.7 | 12 | 19.6 | 9.80 | 27.0 | 90/48 |
| 0.92 | 0.2 | 100 | 147 | 200 | 0.90 | 7.7 | 12 | 19.7 | 1.97 | 0.09 | 90/48 |
| 0.92 | 0.2 | 100 | 121 | 159 | 0.90 | 7.7 | 12 | 21.8 | 2.18 | 0.40 | 90/48 |
| 0.92 | 0.2 | 100 | 176 | 210 | 0.95 | 7.7 | 12 | 29.2 | 1.46 | 0.11 | 90/48 |
| As-received CF-8M Specimen (Heat No. 75) Containing 27.8% Ferrite | | | | | | | | | | | |
| 0.13 | 6.2 | 0 | 258 | 332 | 0.95 | 7.7 | 12 | 25.3 | 1.26 | <0.02 | 93/2 |
| 0.16 | 5.3 | 0 | 240 | 317 | 0.95 | 7.7 | 12 | 34.7 | 1.73 | 1.6 | 93/2 |
| 0.14 | 7.0 | 0 | 242 | 296 | 0.95 | 7.7 | 12 | 35.2 | 1.76 | 1.8 | 93/2 |
| 0.13 | <0.002 | 0 | -560 | -580 | 0.95 | 7.7 | 12 | 35.2 | 1.76 | <0.02 | 93/2 |
| 0.18 | 0.3 | 0 | 198 | 243 | 0.95 | 7.7 | 12 | 36.4 | 1.82 | 1.4 | 93/2 |
| 0.11 | 1.1 | 0 | 216 | 260 | 0.95 | 7.7 | 12 | 36.8 | 1.84 | 1.5 | 93/2 |
| 0.11 | 0.9 | 0 | 206 | 257 | 1.0 | 0 | ∞ | 36.8 | 0 | <0.02 | 93/2 |
| 0.10 | 7.2 | 0 | 247 | 301 | 0.95 | 7.7 | 12 | 45.6 | 2.28 | 2.5 | 93/2 |
| Aged[f] CF-8M Specimen (Heat No. 75) Containing 27.8% Ferrite | | | | | | | | | | | |
| 0.13 | 6.2 | 0 | 258 | 332 | 0.95 | 7.7 | 12 | 24.7 | 1.23 | 4.4 | 93/2 |
| 0.16 | 5.3 | 0 | 240 | 317 | 0.95 | 7.7 | 12 | 37.2 | 1.86 | 8.1 | 93/2 |
| 0.14 | 7.0 | 0 | 242 | 296 | 0.95 | 7.7 | 12 | 46.0 | 2.30 | 19.6 | 93/2 |
| 0.13 | <0.002 | 0 | -560 | -580 | 0.95 | 7.7 | 12 | 46.0 | 2.30 | <0.02 | 93/2 |
| 0.18 | 0.3 | 0 | 198 | 243 | 0.95 | 7.7 | 12 | 47.5 | 2.38 | 1.1 | 93/2 |
| 0.11 | 1.1 | 0 | 216 | 260 | 0.95 | 7.7 | 12 | 53.6 | 2.68 | 7.3 | 93/2 |
| 0.11 | 0.9 | 0 | 206 | 257 | 1.0 | 0 | ∞ | 61.4 | 0 | 20.8 | 93/2 |
| Aged[g] CF-8M Specimen (Heat No. 75) Containing 27.8% Ferrite | | | | | | | | | | | |
| 0.07 | 4.4 | 0 | 256 | 280 | 0.80 | 7.7 | 12 | 31.8 | 6.36 | 58.0 | 93/27 |
| 0.08 | 4.3 | 0 | 237 | 243 | 0.90 | 7.7 | 12 | 33.1 | 3.31 | 16.2 | 93/27 |
| 0.07 | 4.2 | 0 | 247 | 301 | 0.70 | 7.7 | 12 | 34.9 | 10.47 | 122.0 | 93/27 |
| 0.07 | 4.5 | 0 | 252 | 337 | 0.30 | 7.7 | 12 | 38.2 | 26.74 | 349.0 | 93/27 |
| 0.11 | 0.43 | 0 | 205 | 218 | 0.90 | 7.7 | 12 | 40.6 | 4.06 | 15.9 | 93/27 |
| 0.07 | 0.60 | 0 | 214 | 223 | 0.70 | 7.7 | 12 | 43.8 | 13.14 | 110.0 | 93/27 |
| 0.11 | 0.50 | 0 | 205 | 211 | 0.30 | 7.7 | 12 | 52.5 | 36.75 | 666.0 | 93/27 |
| As-received CF-8 Specimen (Heat No. 68) Containing 27.8% Ferrite | | | | | | | | | | | |
| 0.07 | 4.4 | 0 | 256 | 280 | 0.80 | 7.7 | 12 | 30.2 | 6.04 | 16.9 | 93/27 |
| 0.08 | 4.3 | 0 | 237 | 243 | 0.90 | 7.7 | 12 | 30.5 | 3.05 | 3.9 | 93/27 |
| 0.07 | 4.2 | 0 | 247 | 301 | 0.70 | 7.7 | 12 | 30.9 | 9.27 | 39.2 | 93/27 |
| 0.07 | 4.5 | 0 | 252 | 337 | 0.30 | 7.7 | 12 | 32.0 | 22.40 | 170.0 | 93/27 |
| 0.11 | 0.43 | 0 | 205 | 218 | 0.90 | 7.7 | 12 | 32.4 | 3.24 | 2.9 | 93/27 |
| 0.07 | 0.60 | 0 | 214 | 223 | 0.70 | 7.7 | 12 | 33.1 | 9.93 | 32.8 | 93/27 |
| 0.11 | 0.50 | 0 | 205 | 211 | 0.30 | 7.7 | 12 | 34.4 | 24.08 | 157.0 | 93/27 |

*Table 7. (Cont'd)*

| Water Chemistry | | | Potentials | | | | | CGR Data | | | |
|---|---|---|---|---|---|---|---|---|---|---|---|
| Cond., µS·cm$^{-1}$ | $O_2$, ppm | $SO_4^{2-}$, ppb | 304 SS, mV(SHE) | Pt, mV(SHE) | Load Ratio | Freq., $10^{-2}$ Hz | Rise Time, s | $K_{max}$[c], MPa·m$^{1/2}$ | ΔK,[d] | Rate, $10^{-10}$ m·s$^{-1}$ | ANL Report No. |
| Aged[f] CF-8 Specimen (Heat No. 68) Containing 27.8% Ferrite | | | | | | | | | | | |
| 0.13 | 6.2 | 0 | 258 | 332 | 0.95 | 7.7 | 12 | 26.0 | 1.30 | <0.02 | 93/2 |
| 0.16 | 5.3 | 0 | 240 | 317 | 0.95 | 7.7 | 12 | 35.0 | 1.75 | 0.42 | 93/2 |
| 0.14 | 7.0 | 0 | 242 | 296 | 0.95 | 7.7 | 12 | 36.9 | 1.85 | 4.6 | 93/2 |
| 0.13 | <0.002 | 0 | -560 | -580 | 0.95 | 7.7 | 12 | 36.9 | 1.85 | <0.02 | 93/2 |
| 0.18 | 0.3 | 0 | 198 | 243 | 0.95 | 7.7 | 12 | 37.4 | 1.87 | 0.93 | 93/2 |
| 0.11 | 1.1 | 0 | 216 | 260 | 0.95 | 7.7 | 12 | 37.8 | 1.89 | 1.4 | 93/2 |
| 0.11 | 0.9 | 0 | 206 | 257 | 1.0 | 0 | ∞ | 37.8 | 0 | <0.02 | 93/2 |
| 0.10 | 7.2 | 0 | 247 | 301 | 0.95 | 7.7 | 12 | 52.5 | 2.62 | 11.3 | 93/2 |
| Aged[g] CF-8 Specimen (Heat No. 68) Containing 27.8% Ferrite | | | | | | | | | | | |
| 0.07 | 4.4 | 0 | 256 | 280 | 0.80 | 7.7 | 12 | 30.9 | 6.18 | 31.9 | 93/27 |
| 0.08 | 4.3 | 0 | 237 | 243 | 0.90 | 7.7 | 12 | 31.3 | 3.13 | 5.4 | 93/27 |
| 0.07 | 4.2 | 0 | 247 | 301 | 0.70 | 7.7 | 12 | 32.1 | 9.63 | 53.7 | 93/27 |
| 0.07 | 4.5 | 0 | 252 | 337 | 0.30 | 7.7 | 12 | 33.0 | 23.10 | 157.0 | 93/27 |
| 0.11 | 0.43 | 0 | 205 | 218 | 0.90 | 7.7 | 12 | 33.6 | 3.36 | 4.2 | 93/27 |
| 0.07 | 0.60 | 0 | 214 | 223 | 0.70 | 7.7 | 12 | 34.4 | 10.32 | 32.4 | 93/27 |
| 0.11 | 0.50 | 0 | 205 | 211 | 0.30 | 7.7 | 12 | 35.8 | 25.06 | 191.0 | 93/27 |

[a] Compact-tension specimens were fabricated from Heat No. F5524 (0.7TCT) and from Heats No. P2, 68, and 75 (1TCT).

[b] Positive sawtooth waveform was used.

[c] Stress intensity, $K_{max}$, value at the end of each time period.

[d] $\Delta K = K_{max}(1 - R)$, where the load ratio $R = K_{min}/K_{max}$.

[e] Sine waveform was used.

[f] Specimens aged for 10,000 h at 400°C.

[g] Specimens aged for 30,000 h at 350°C.

As mentioned previously, thermal aging embrittlement is caused by precipitation and growth of a Cr-rich α′ phase, a Ni- and Si-rich G phase, $M_{23}C_6$, γ (austenite) in the ferrite, and additional precipitation and/or growth of existing carbides at the ferrite/austenite phase boundaries. These compositional changes increase the tensile strength and decrease the impact energy and fracture toughness of the steels, where, in general, the Mo-free grades (CF-3 and -8) are more resistant and the Mo-bearing (CF-3M and -8M) grades are less resistant to thermal embrittlement. The tensile properties[35] of the various steels in the as-received and thermally aged conditions at 289°C are shown in Table 8. Tensile properties of wrought Types 304[42] and 316NG[43] SS are also included in the table. To determine whether corrosion-fatigue behavior of the steels in high-temperature water can be correlated with the thermal aging characteristics, the CGRs under high-R loading were plotted versus the square of yield stress $\sigma_y$ for specimens of the same heats under identical aging conditions (time and temperature). The limited results in Fig. 23 indicate a linear relationship between the CGRs and $\sigma_y^2$ in water containing 4-8 and 0.2-0.4 ppm DO, within the uncertainty of the experimental data. Data for wrought grades of Types 304 and 316NG SS are also included in the figures (solid symbols).[44]

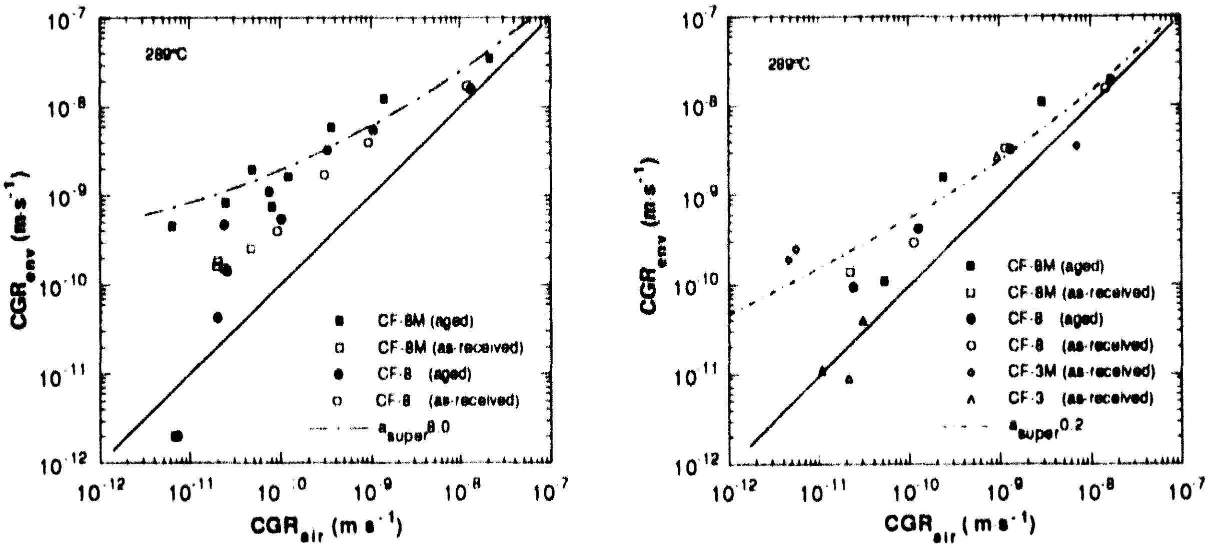

*Figure 22. Corrosion fatigue data for as-received CF-3, -3M, and -8M and aged CF-8M and -8 cast SS in water containing 8 (left) and 0.2 (right) ppm DO at 289°C. Diagonal lines correspond to crack growth in air in Section XI of the ASME Code. Dashed lines indicate predictions from a correlation for wrought SS.*[41]

*Table 8. Tensile properties of wrought and cast SSs at 289°C*

| Material | Heat No. | Aging Conditions | | Tensile Properties | | | | | Ref. No. |
|---|---|---|---|---|---|---|---|---|---|
| | | Time (h) | Temp. (°C) | $\sigma_u$ (MPa) | $\sigma_y$ (MPa) | $\varepsilon_T$ (%) | RA[a] (%) | H[b] (MPa) | |
| 304 SS | 30956 | Solution-Annealed | | 512.0 | 152.0 | 53.0 | 77.0 | 679.2 | 42 |
| CF-8 | 68 | As-Received | | 412.3 | 156.4 | 37.9 | 60.6 | 675.1 | 35 |
| CF-8 | 68 | 10,000 | 400 | 475.6 | 176.7 | 34.4 | 47.6 | 868.9 | 35 |
| CF-8 | 68 | 30,000 | 350 | 427.3 | 190.4 | 25.3 | 41.7 | 936.4 | 35 |
| 316NG | P91576 | Solution-Annealed | | 466.0 | 142.0 | 29.0 | 64.0 | 1117.2 | 43 |
| CF-8M | 75 | As-Received | | 474.8 | 191.5 | 30.5 | 45.0 | 928.9 | 35 |
| CF-8M | 75 | 10,000 | 400 | 630.4 | 208.2 | 23.7 | 31.4 | 1781.4 | 35 |
| CF-8M | 75 | 30,000 | 350 | 615.9 | 264.4 | 23.0 | 30.2 | 1528.3 | 35 |

[a] Reduction in area.

[b] Strain-hardening coefficient ; $H = (\sigma_u - \sigma_y)/\varepsilon_T$.

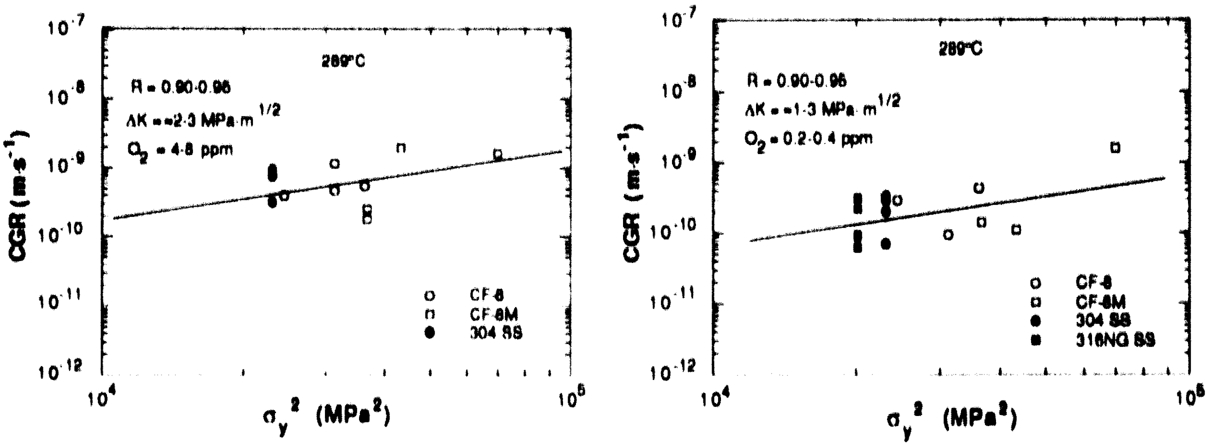

*Figure 23. Dependence of CGRs of as-received and thermally aged CF-8 and -8M cast SS on yield stress of the materials at 289°C under high-R loading in water containing 4-8 (left) and 0.2-0.4 (right) ppm DO. Solid symbols denote wrought Types 304 and 316NG SS.*

In the case of pure mechanical fatigue, where environmental effects are absent, the CGR da/dN (m/cycle) can be written as[45]

$$\frac{da}{dN}=\left(\gamma_f-\gamma_r\right)r_p\cos\theta \tag{3}$$

where $\gamma_f$ and $\gamma_r$ are the the average plastic strain in forward and reverse slip, $\theta$ represents the favorably oriented slip direction within the plastic zone, and $r_p$ is the cyclic plastic zone size,[46]

$$r_p=\frac{1}{3\pi}\left(\frac{\Delta K}{2\sigma_y}\right)^2 \tag{4}$$

and $\Delta K = K_{max} - K_{min}$ and $\sigma_y$ is the yield stress. The time-base CGR da/dt ($m{\cdot}s^{-1}$) is given by

$$\frac{da}{dt}=\frac{da}{dN}\left(\frac{1}{t_r}\right)=\frac{\left(\gamma_f-\gamma_r\right)}{t_r}\frac{1}{3\pi}\left(\frac{\Delta K}{2\sigma_y}\right)^2\cos\theta \tag{5}$$

where $t_r$ is the rise time (s) of the positive sawtooth wave form. When strain hardening of the material is considered,[45] the CGR compensated for strain hardening can be written as

$$H\frac{da}{dt}=H\frac{da}{dN}\left(\frac{1}{t_r}\right)=\frac{\beta}{t_r(1-R)}\frac{(\Delta K)^3}{\sigma_y^2} \tag{6}$$

where $\beta$ is parameter that combines several microstructural and geometric factors, R is the load ratio $K_{min}/K_{max}$, and H is the strain-hardening coefficient

$$H=\frac{\sigma_u-\sigma_y}{\varepsilon_t} \tag{7}$$

where $\sigma_u$ and $\sigma_y$ are the ultimate tensile and the yield strengths, respectively, and $\varepsilon_t$ is the total strain at failure of the material.

In the absence of any environmental effect on crack growth at a constant rise time and $\Delta K$ in the Paris regime (power law exponent for $\Delta K$ of ≈3), Eq. 6 indicates that the strain-hardening-compensated CGRs, H(da/dt), should decrease as the yield strength increases following a $1/\sigma_y^2$ dependence, i.e., a logarithmic plot of H(da/dt) versus $\sigma_y^2$ would have a slope of −1. Although data for the dependence of CGRs on yield stress are sparse, CGRs (compensated for the strain-hardening behavior) of an 0.5Cr-0.5Mo-0.25V steel with different heat treatments, which produce a range of yield strengths, follow this type of dependence in air at ambient temperature.[45,47]

In the present tests on as-received and thermally aged cast SSs in high-temperature oxygenated water, the strain-hardening-compensated CGRs tend to increase as the yield strength increases, as shown in Fig. 24. The lines on each plot in Figs. 23 and 24 represent a slope of 1, which indicate that the CGRs in oxygenated water, as well as those compensated by the strain-hardening coefficient, are proportional to $\sigma_y^2$, in contrast to $1/\sigma_y^2$ in the case of pure mechanical fatigue of the ferritic steel in air.

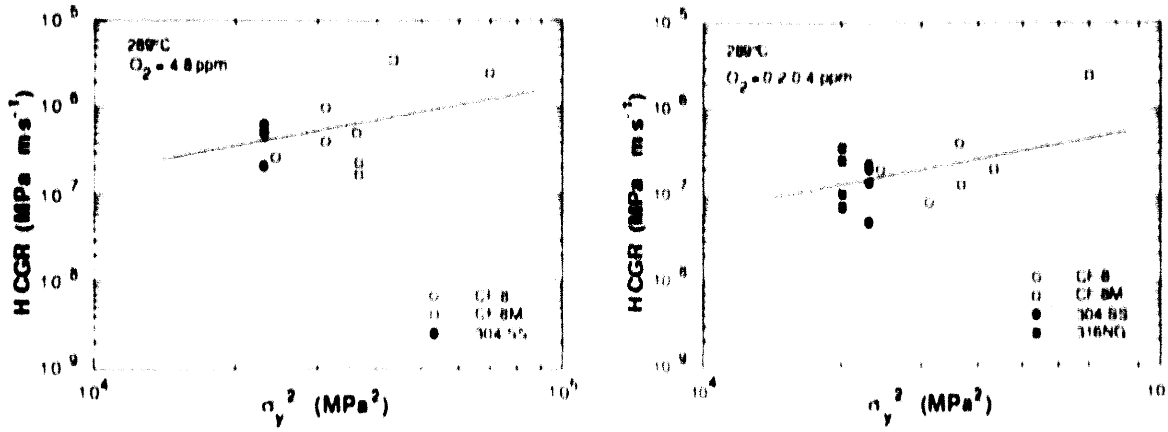

*Figure 24. Dependence of strain-hardening-compensated CGRs of as-received and thermally aged CF-8 and -8M cast SS on yield stress of the materials at 289°C under high R loading in water containing 4-8 (left) and 0.2-0.4 (right) ppm DO. Solid symbols denote wrought Types 304 and 316NG SS.*

Fracture mechanics CGR tests are in progress on other heats of cast SS to determine the effects of thermal aging on corrosion fatigue behavior over a wider range of loading conditions.

## 4 Irradiation-Assisted Stress Corrosion Cracking of Austenitic SS

In recent years, failures of reactor-core internal components in both BWRs and PWRs have increased after accumulation of relatively high fluence (>5 x $10^{20}$ n·cm⁻², E >1 MeV). The general pattern of the observed failures indicates that as nuclear plants age and neutron fluence increases, various apparently nonsensitized austenitic SSs become susceptible to intergranular failure. Some components (e.g., BWR control blade handle and sheath) are known to have cracked under minimal applied stress. Although most failed components can be replaced, some safety-significant structural components, such as the BWR top guide, shroud, and core plate, would be very difficult or impractical to replace.

Therefore, the structural integrity of these components after accumulation of high fluence has been a subject of concern, and extensive research has been conducted to provide an understanding of this type of degradation, which is commonly known as irradiation-assisted stress corrosion cracking (IASCC).

In the mid 1960s, investigators began to implicate impurities such as Si, P, and S in IASCC failure of fuel cladding fabricated from solution-annealed nonsensitized austenitic SS.[48-52] Since then, it seems that the concept of superior resistance of HP materials of SSs low in Si, P, S, and C has proved valid after the favorable experience with HP Type 348 SS fuel cladding in the La Crosse BWR[53] and the subsequent demonstration of superior performance of the low-N HP 348 SS heat from swelling tube tests in a BWR and PWR.[54-55] Although data were very limited, results from a laboratory slow-strain-rate-tensile (SSRT) tests[56] also suggest superior performance of the same HP heat of Type 348 SS investigated in Refs. 53-55. The better performance seemed to indicate that radiation-induced segregation (RIS) of Si is the predominant process, because RIS of other impurities and Cr depletion in the HP and CP Type 348 SS were either similar or could not be detected by field emission gun scanning transmission electron microscopy (FEG-STEM).[56] It has also been reported that Type 316L SS, irradiated in the mixed-spectrum Advanced Test Reactor (ATR), exhibited better resistance to SCC than Type 316NG SS,[57] indicating a possible benefit of low N. On the basis of this experience with Types 348 and 316 SS, HP Type 304 SS has been suggested as a better alternative to CP Type 304 SS, which has been used to fabricated the majority of core internal components of operating BWRs and PWRs. Recently, Jacobs reported that BWR neutron absorber tubes (QC-AT, Table 9) fabricated from one HP heat of Type 304 SS (HP304-CD, Table 9) performed better than similar counterparts fabricated from CP Type 304 SS materials under conditions of nonereviced water chemistry.[58]

However, in direct contradiction of the above experiences, results from SSRT tests conducted on several other BWR neutron absorber tubes indicate that SCC resistance of other HP heats of Type 304 SS is worse than that of CP materials.[59,60] Results consistent with this observation have also been reported for Type 304 SS specimens irradiated by either neutrons,[61] ions,[62] or protons.[63] Therefore, the issue of superior performance of HP materials and the mechanisms of IASCC appear to be far from established. Nevertheless, one important point seems to be quite clear; that is, heat-to-heat variation in susceptibility to IASCC can be significant, even among HP materials containing virtually identical chemical compositions. This seems to cast serious doubt not only on the role of grain boundary segregation of impurities (i.e., Si, P, or S) but also on the premise that Cr depletion is the primary mechanism of IASCC.

In the present study, a comparative analysis of grain boundary microchemistry was conducted on a unique pair of BWR neutron absorber tubes of virtually identical chemical composition but exhibiting a significant difference in susceptibility to IGSCC in SSRT tests. One of the neutron absorber tubes (QC-AT, Table 9) was fabricated from the HP heat (HP304-CD), which exhibited superior in-reactor performance reported by Jacobs et al.;[58] the other neutron absorber tube (V-AT) was fabricated from a similar HP heat (HP304-A) but exhibited a relatively high susceptibility to IGSCC during SSRT tests.[59,60] SSRT tests independent of those in Refs. 59 and 60 were conducted on both materials, and the results showed that IGSCC susceptibility of the former material (QC-AT) was lower than that of the latter (V-AT) for a similar fluence level.* Chemical compositions of the two materials were virtually identical except for N and B contents. Therefore, a comparative analysis of the two materials was considered to be ideal for investigating the significant difference in susceptibility to IGSCC. The objective of this study was to identify the cause of the strong heat-to-heat variation of the HP materials, thereby providing an important clue to the primary process that influences IASCC of austenitic SSs.

## 4.1 Susceptibility to Intergranular Cracking in Water and in Vacuo

**(H. M. Chung, W. E. Ruther, and J. E. Sanecki)**

Specimen preparation, procedures for SSRT tests, and a description of the hot-cell SSRT apparatus were given in previous reports.[59,60] Cylindrical tensile specimens were sectioned from top-, middle-, and bottom-axial positions of neutron-absorber-rod tubes fabricated from several CP and HP heats of Type 304 SS and irradiated in several BWRs. Boron carbide absorber was removed with carbide-tip drills. Tensile specimens, fabricated from BWR control-blade sheaths, were also tested. SSRT tests were conducted in air and in simulated BWR water at 289°C at a strain rate of $1.65 \times 10^{-7}$ $s^{-1}$. The DO concentration and conductivity of the simulated BWR water were ≈0.3 ppm and 0.12 $\mu S \cdot cm^{-1}$, respectively. Fracture surface analysis of SSRT specimens was conducted by SEM to determine the types of fracture surface morphology.

The fast-neutron fluence and chemical composition of the HP and CP heats of Type 304 SS are given in Table 9. Chemical compositions of the three HP heats are similar except for N and B contents. Boron content could not be determined accurately at levels of <0.001 wt.%. However, Heat HP304-CD had a higher boron content than did Heats HP304-A or -B.

Grain boundary microchemistry was analyzed with a JEOL Model JAMP-10 scanning Auger microscope (SAM). Specimens charged with hydrogen were fractured at room temperature in the high vacuum (~7 to 20 × $10^{-7}$ Pa) of the SAM to reveal IG fracture surfaces. Hydrogen was charged into the notched AES specimens for 48 h at 60°C in a solution of 100 mg/L $NaAsO_2$ dissolved in 0.1N $H_2SO_4$ at a current density of 500 $mA \cdot cm^{-2}$. IG fracture of the hydrogen-charged specimens was observed in bands below the free surface of the vacuum-fractured specimen. Average penetration depth of the more-or-less uniform IG fracture bands was measured in each specimen. A Cr depth profile was obtained as a function of sputter distance beneath a selected region of IG fracture. Details of the procedure are given in Ref. 60.

The percent IGSCC measured in the specimens from BWR components has been plotted as a function of fast-neutron fluence and yield strength in Figs. 25A and 25B, respectively. Similar results reported by Jacobs et al.,[57] and Kodama et al.,[64] and Asano et al.[65] are also shown in the figures. All data in Fig. 25A were obtained from BWR components at a strain rate of ~2 × $10^{-7}$ $s^{-1}$ in water containing ~0.3 ppm DO. Figure 25A indicates that IGSCC susceptibility of the CP control blade sheath is significantly lower than that of the CP neutron absorber tube or the dry tube of Kodama et al.[64] for comparable

---

* A. J. Jacobs, General Electric Co., private communications, 1993.

fluence level. The susceptibility of the HP absorber tube is greater than that of any of the CP materials.

*Table 9. Chemical composition and fluence of HP and CP Type 304 SS BWR components*

| Heat ID No | Composition (wt.%) Cr | Ni | Mn | C | N | B | Si | P | S | Source Code | Service Reactor | Fluence $10^{21}$ n cm$^{-2}$ |
|---|---|---|---|---|---|---|---|---|---|---|---|---|
| HP304-A | 18.50 | 9.45 | 1.81 | 0.018 | 0.100 | <0.001 | <0.03 | 0.005 | 0.003 | V-AT[a] | BWR-B | 0.2-1.4 |
| HP304-B | 18.30 | 9.75 | 1.32 | 0.015 | 0.080 | <0.001 | 0.05 | 0.005 | 0.005 | V-AT[a] | BWR-B | 0.2-1.4 |
| HP304-CD | 18.58 | 9.44 | 1.22 | 0.017 | 0.037 | 0.001 | 0.02 | 0.002 | 0.003 | V-AT[a] | BWR-B | 0.2-1.4 |
| HP304-CD | 18.58 | 9.44 | 1.22 | 0.017 | 0.037 | 0.001 | 0.02 | 0.002 | 0.003 | QC-AT[a] | BWR-QC | 2.0 |
| CP304-A | 16.80 | 8.77 | 1.65 | 0.08[b] | 0.052 | – | 1.55 | 0.045[b] | 0.030[b] | HL-AT[c] | BWR-Y | 0.2-2.0 |
| CP304-B | 18.0-20.0 | 8-10.5 | 2.00[b] | 0.08[b] | | – | 1.00[b] | 0.045[b] | 0.030[b] | LC-S[d] | BWR-LC | 0.5-2.0 |

[a] High-purity neutron absorber tubes, OD = 4.78 mm, wall thickness = 0.63 mm, composition before irradiation.
[b] Represents maximum value in the specification; actual value not measured.
[c] Commercial-purity absorber tubes, OD = 4.78 mm, wall thickness = 0.79 mm, composition after irradiation.
[d] Commercial-purity control blade sheath, thickness 1.22 mm, actual composition not measured.

Apparently, no good correlation is observed between percent IGSCC and yield strength (Fig. 25B). For example, the CP Type 304 SS sheath from the La Crosse BWR exhibits excellent resistance to IG cracking despite unusually pronounced irradiation hardening. The rationale for implicating yield strength is that IASCC may be controlled primarily by irradiation hardening within grains rather than by a process that promotes stress corrosion at the grain boundaries. However, the results in Fig. 25B indicate that although irradiation-induced hardening promotes IGSCC by rendering plastic deformation within grains more difficult as fluence increases, a certain grain boundary process is essential to induce IGSCC in irradiated materials.

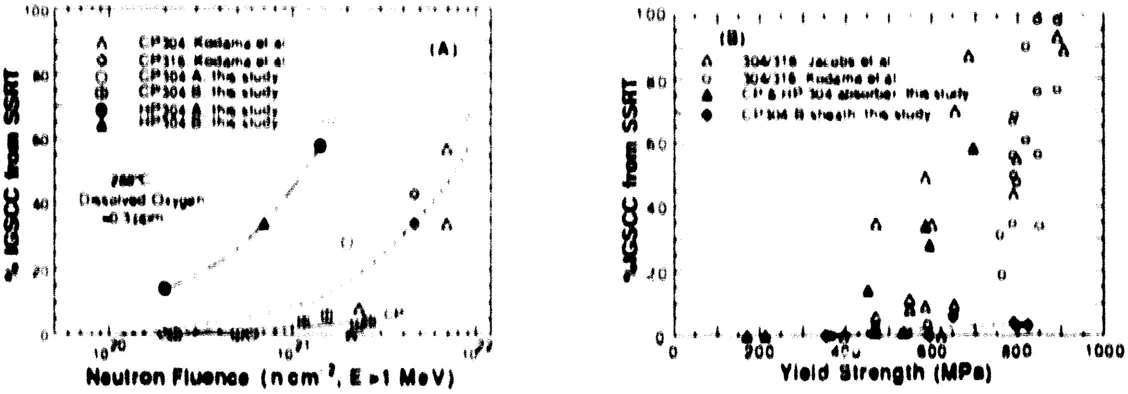

*Figure 25. Percent IGSCC vs. fluence (A) and vs. yield strength (B) for HP and CP Type 304 SS and CP 316 SS BWR components from SSRT tests at 289°C in simulated BWR water*

## 4.2 Effect of Grain-Boundary Microchemistry (H. M. Chung, W. E. Ruther, and J. E. Sanecki)

### 4.2.1 Effects of Si, P, and S

In Fig. 26, the percent IGSCC from the SSRT tests in water has been plotted as function of grain-boundary concentration of Si and P. Data for grain-boundary segregation of Si, P, and other impurities have been reported in Refs. 59 and 60. In the figure, the depth of IG-fracture penetration, produced in hydrogen-charged specimens in vacuo at 25°C, has been also plotted. The X(59-eV) peak shown in Fig. 26C is produced by the secondary Auger electrons of Li and Ni. A more detailed analysis of the identification of the peak is given below. No evidence of segregation of S was observed.[60]

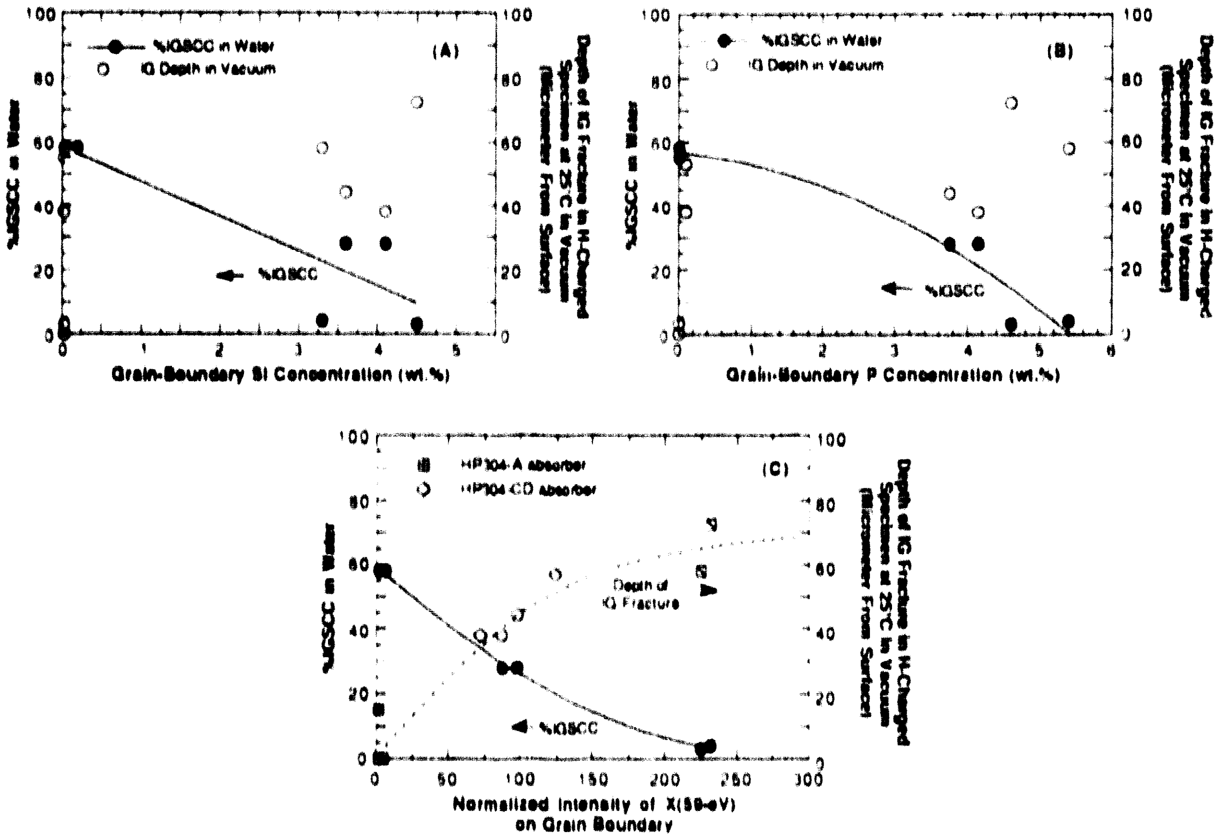

*Figure 26. Percent IGSCC in water and depth of IG fracture penetration in hydrogen-charged specimens, fractured at 25°C in vacuo, as a function of grain-boundary segregation of Si (A), P (B), and X (59-eV) (C). Fluence level of the specimens was ≈2 x $10^{21}$ n·cm$^{-2}$.*

No good correlation was observed between the susceptibility to hydrogen-enhanced IG cracking and grain-boundary concentration of Si or P. Percent IGSCC in water decreases monotonically for increased grain-boundary concentrations of Si, P, and X(59-eV). It is difficult, therefore, to explain the significant IGSCC in the HP absorber tube specimens or the negligible SCC susceptibility of the CP sheath specimens on the basis of grain-boundary segregation of Si, P, or S. The present results show convincingly that grain–boundary segregation of Si, P, or S is not the mechanism of IASCC in Type 304 SS, as has been speculated up to now. Furthermore, the results also strongly imply that low Si, P, and S content is not the primary factor associated with the superior resistance of the HP Type 348 SS reported in Refs. 53–56.

### 4.2.2 Effect of Cr Depletion

Minimum Cr content on grain boundaries of the CP and HP absorber tubes and control-blade sheath was determined from AES depth-profile data, and the values were correlated with percent IGSCC in Fig. 27. In the figure, similar results obtained from the FEG-STEM technique[56,65,66] are also plotted for comparison. The latter results were obtained on SSRT specimens tested in simulated BWR water containing 8–32 ppm of dissolved oxygen. For a better comparison, the percent IGSCC from the present SSRT tests in water with ≈0.3 ppm dissolved oxygen was extrapolated to an oxygen content of 8–32 ppm according to the trend reported by Kodama et al.[64] A comparison similar to that in Fig. 27 has been discussed by Bruemmer et al.[67]

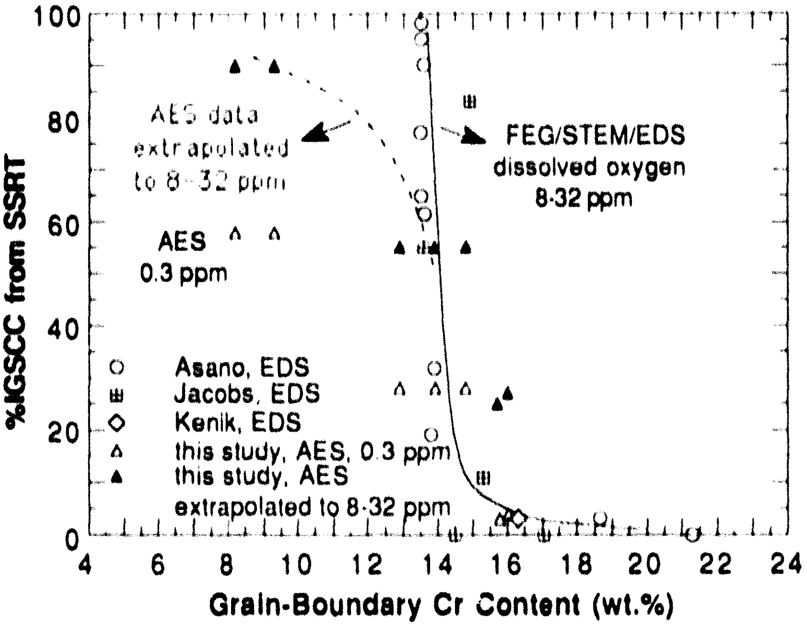

*Figure 27. Percent IGSCC from SSRT tests vs. minimum grain-boundary Cr content determined from AES and FEG STEM analyses of BWR components*

Results of analyses by the two techniques appear to be consistent except for the HP Heat HP304-A, in which the Cr depletion profile is extremely narrow and deep according to AES. A more direct comparison has been reported elsewhere.[60] Figure 27 lends itself to several interpretations; one is that present-generation FEG-STEM referred to in Fig. 27 has limitations in detecting Cr at a concentration of <14 wt.% within ≈1.5 nm of a grain boundary in BWR-irradiated materials. This may be because of several inevitable limitations associated with the energy-dispersive spectroscopy (EDS) technique in present-generation FEG-STEM, i.e., effects of imperfect grain-boundary alignment (1-nm uncertainty from 1° misalignment in a 57-nm thick film), the relatively large beam size (≈2.5 nm),[68,69] beam broadening,[68,69] the effect of the $Cr_2O_3$ surface layer, and fluoresced Cr X-ray.[56] Because of these limitations, practical resolution of the present-generation FED-STEM-EDS analysis should be considered close to 3.5-4 nm. The resolution limit can be greatly improved by utilizing the technique of electron-energy-loss spectroscopy (EELS) instead of EDS.[69] AES data can also be influenced by oxygen contamination from the microscope vacuum environment.

Without a proper understanding of the limitations of the techniques and uncertainties of the measurements, and in the absence of a more convincing database (e.g., data from EELS in a next-generation FEG-STEM), the role of grain-boundary Cr depletion cannot be determined convincingly at present. Based on either FEG-STEM or AES data, Fig. 27 suggests that for <30% IGSCC, susceptibility is influenced significantly by Cr depletion. However, the seemingly strong increase in percent IGSCC despite the nearly constant grain-boundary Cr content of ≈14-15 wt.% (FEG-STEM data) implies that an unidentified process other than Cr depletion plays an important role. According to AES data, Cr depletion plays an important role even for >50% IGSCC.

### 4.2.3 Comparative Analysis of Similar High-Purity Heats

To provide a clue to the question of whether one or more unidentified processes play an important role in IASCC, a case study was conducted using absorber tube specimens that were fabricated from two virtually identical HP heats (HP304-A, less resistant to IGSCC during SSRT,[59,*] and HP304-CD, more resistant to IGSCC/SSRT)[*] irradiated to a fluence level of ≈$2.0 \times 10^{21}$ n·cm$^{-2}$. The rationale was that because Si, P, S, C, Ni, Cr, Mn, and fluence levels were similar in the two heats, grain-boundary concentrations of these elements and irradiation-induced hardening should be similar. Therefore, it should be relatively easy to identify other aspects of grain-boundary chemistry that could be correlated with resistance to IGSCC. The two materials also exhibited a surprisingly large difference in their susceptibilities to IG fracture in vacuo after H-charging (see Fig. 26C). In contrast to HP304-CD, it was very difficult to produce IG fracture in vacuo in H-charged specimens of HP304-A, a trend opposite to susceptibility to IGSCC in water. Grain-boundary Cr depletion in the two specimens, determined by AES depth-profiling, is shown in Fig. 28. Not surprisingly, Cr depletion in the specimens was similar because of a virtually identical chemical composition and similar fluence.

Grain-boundary segregation behavior of Ni and impurities in the two specimens is summarized in Fig. 29. In the figure, segregation behavior of Ni, Si, P, C, S, N, X(59-eV), and B can be determined by comparing intensities of the elements on ductile (denoted "D") and intergranular (denoted "I") fracture surfaces. The left- and right-hand columns of Fig. 29 show results measured on HP304-A and HP304-CD specimens, respectively. In Fig. 30, duplicate results obtained from another specimen of HP304-CD are shown. Whenever grain-boundary segregation is clearly indicated for a given element, a horizontal line shows the average intensity of the element on grain boundaries, e.g., Ni in HP304-A (Fig. 29A). In the HP304-A specimen, only Ni segregation was evident. In the HP304-CD specimen, grain-boundary segregation of not only Ni but N, X(59-eV), and B was evident. Figures 29H and 30D indicate segregation of C in the two specimens of HP304-CD, but the evidence seems less convincing.

---

[*] A. J. Jacobs, General Electric Co., private communications, 1993.

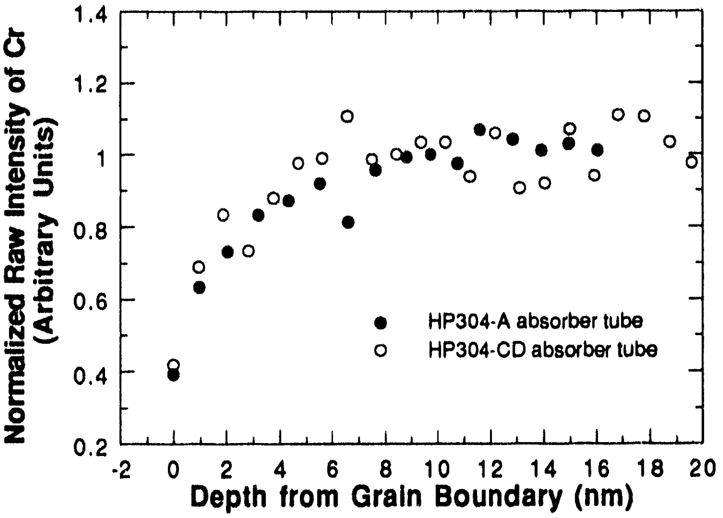

*Figure 28. Comparison of grain-boundary Cr-depletion profiles determined from AES analyses of HP304-A and HP304-CD absorber tubes irradiated to 2 x $10^{21}$ n·cm$^{-2}$*

### 4.2.4 Identification of Li on Grain Boundaries

To identify the X(59-eV) peak, Auger spectra were obtained from several types of CP Type 304 SS specimens, i.e., irradiated, nonirradiated, and corroded in liquid Li (because this element, which is produced by thermal-neutron transmutation of $_5B^{10}$, may contribute to the peak). The results are summarized in Fig. 31. The X(59-eV) peak was observed in Auger spectra obtained from: (a) irradiated Type 304 SS BWR components (Fig. 31D), (b) nonirradiated Type 304 SS specimens that were corroded in liquid lithium at 600°C for 144 h (Fig. 31B), nonirradiated Type 310 SS containing 20 wt.% Ni (Fig. 31C), and (c) nonirradiated Type 330 SS containing 35 wt.% Ni. The characteristic shape of the peak observed in nonirradiated Type 310 SS was somewhat different from those observed in the Li-corroded, nonirradiated, and irradiated Type 304 SS specimens. The peak was absent in nonirradiated specimens of Types 304, 347, AISI 3340, and martensitic SS, as shown more quantitatively in Fig. 32.

These results show that at least some fraction of the intensity of the X(59-eV) peak observed in specimens of HP304-CD (Figs. 29O and 30G) is due to Li. Results in Figs. 29A, 29E, and 30A show that Ni-segregation ratios in the HP304-A and HP304-CD specimens are virtually identical. Because the bulk concentration of Ni is virtually the same (i.e., 9.45 wt.%; see Table 9), the grain-boundary concentration of Ni in the two specimens should be similar. Accordingly, it is difficult to attribute the large difference in the intensity of X(59-eV) between HP304-A (Fig. 29K) and HP304-CD (Fig. 29O) to grain-boundary concentrations of Ni. The segregation behavior of X(59-eV) (Figs. 29O and 30G) and B (Figs. 29P and 30H) in HP304-CD was also similar. Therefore, we conclude that the X(59-eV) peak observed on the grain boundaries of HP304-CD is in fact the secondary peak (≈58 eV) of Li, whereas the primary peak of Li (≈43 eV) was superimposed on the 47-eV peak of Fe.

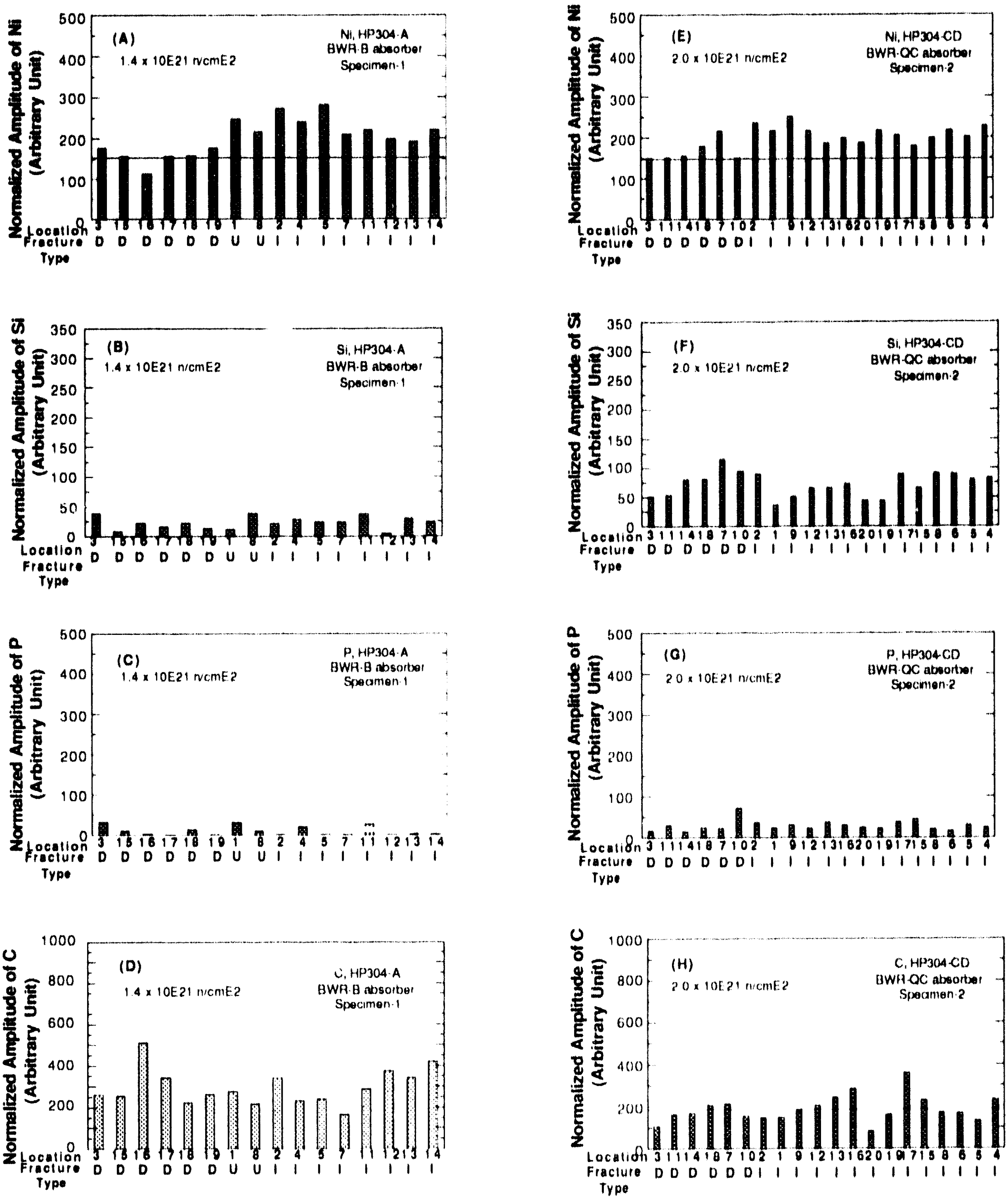

*Figure 29.* *Intensities of Ni, Si, P, and C signals from ductile (denoted by "D"), intergranular ("I"), and faceted ("U") fracture surfaces of neutron absorber tubes fabricated from the HP heats HP304-A (A to D) and HP304-CD (E to H) and irradiated to ≈1.4 x $10^{21}$ and ≈2.0 x $10^{21}$ n·cm$^{-2}$, respectively. Intensities of S, N, X (59 eV), and B signals from the HP heats HP304-A (I to L) and HP304-CD (M to P).*

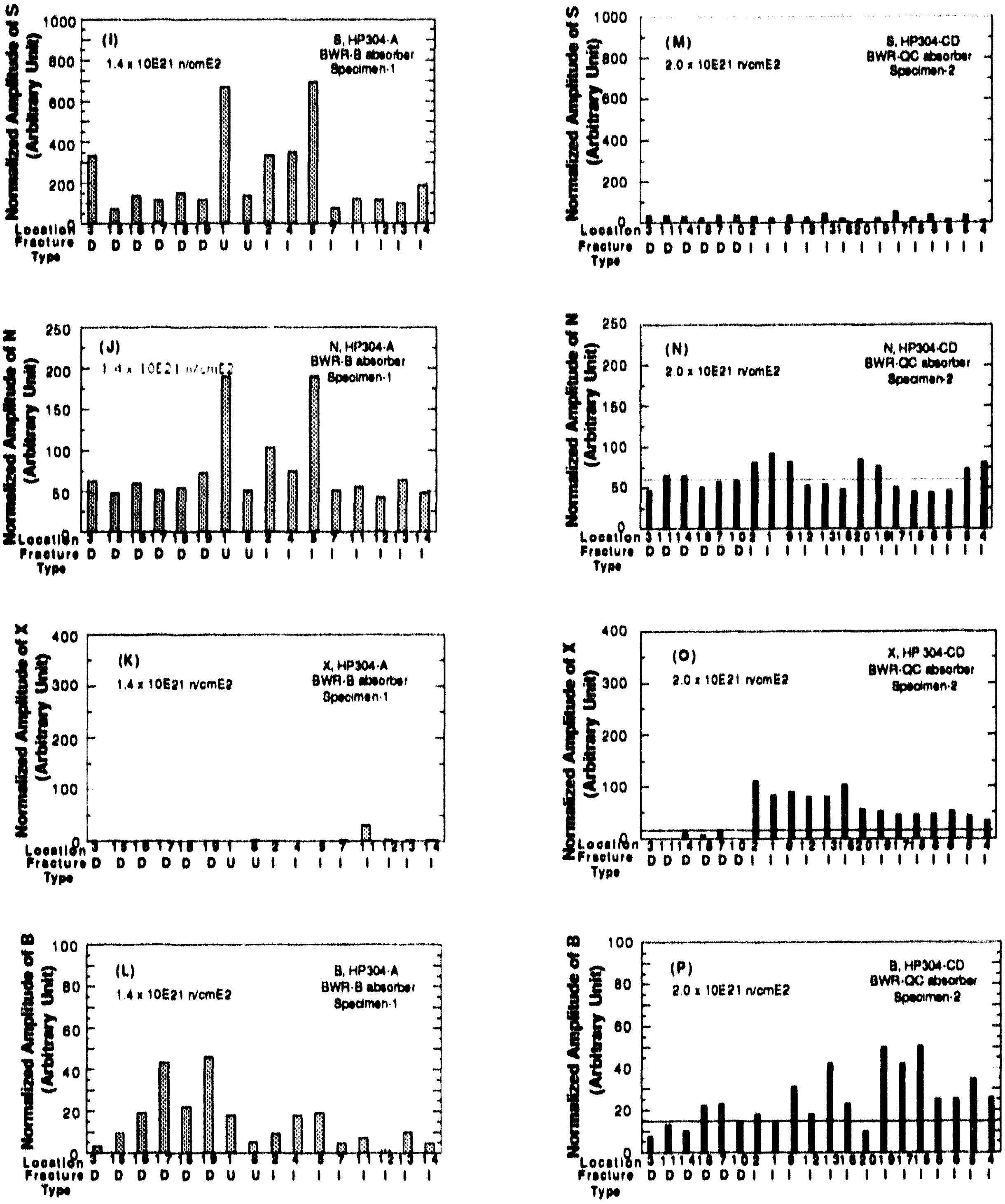

*Figure 29. (Cont'd)*

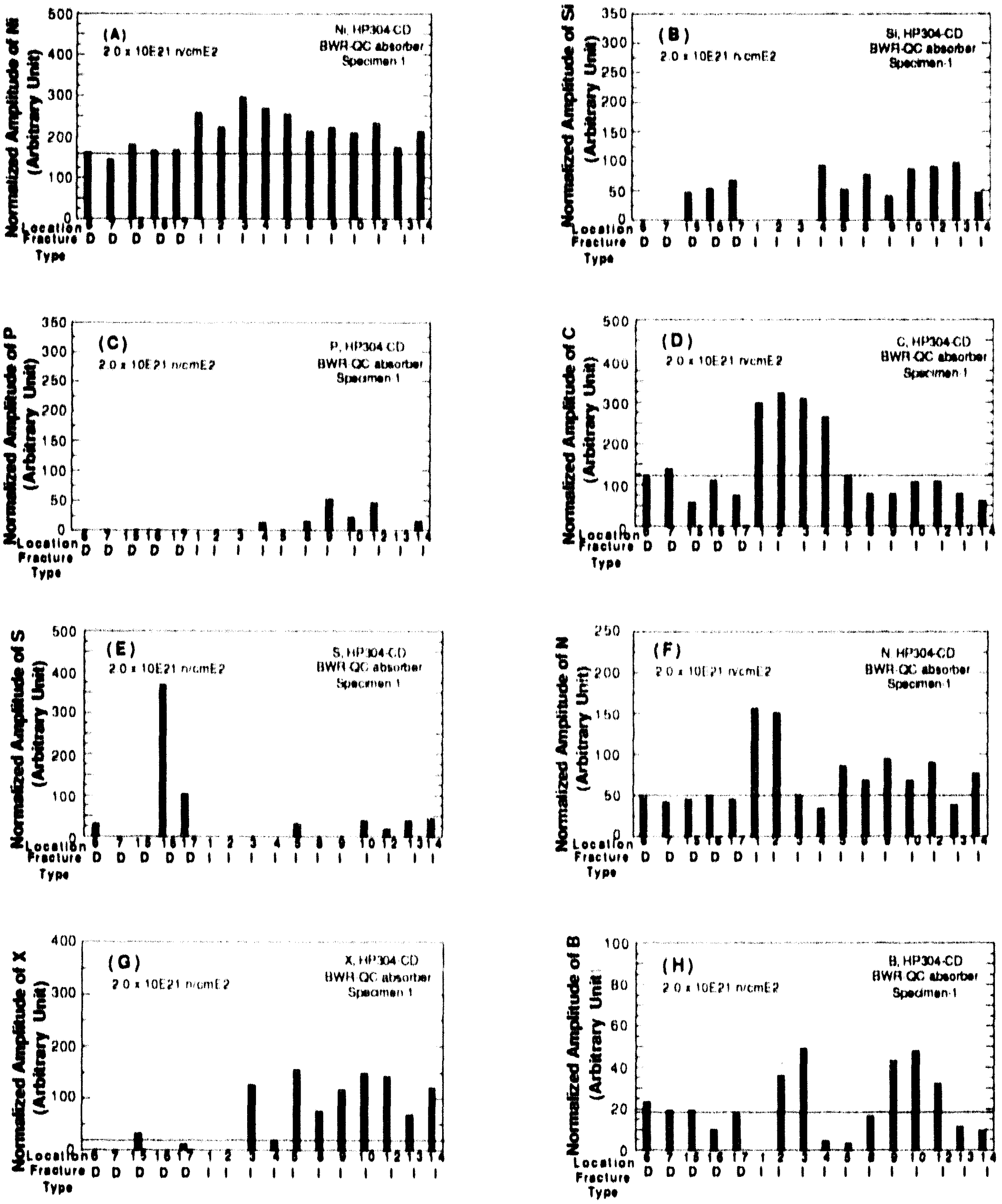

*Figure 30. Intensities of Ni, Si, P, C, S, N, X (59 eV), and B signals (A to H) from ductile (denoted by "D"), intergranular ("I"), and faceted ("U") fracture surfaces of a duplicate specimen of neutron absorber tube fabricated from HP heat HP304 CD and irradiated to ≈2.0 x $10^{21}$ n·cm$^{-2}$*

As was mentioned previously, Li is produced from transmutation by thermal neutrons of $^{10}B$ dissolved in the BWR specimens, i.e., $^{10}B(n, He)^7Li$. The cross section for this reaction is large, i.e., ≈3840 barn. Natural B dissolved in the absorber tubes is composed of 19.8% $^{10}B$ and 80.2% $^{11}B$. However, it is not clear if one can rule out the possibility that some of the Li atoms detected in the absorber rod tubes came from the $B_4C$ absorber that is enriched in $^{10}B$.

Boron in austenitic steels is known to segregate strongly to grain boundaries by thermal processes. Therefore, grain-boundary concentrations of B, and hence Li, could be influenced during fabrication of the absorber tubes, even if the tubes were extruded from the same starting material. During slow cooling of thick sections (e.g., a BWR top guide), thermal segregation of B is likely to be more pronounced. When segregated $^{10}B$ transmutes to Li and helium, Li will be scattered away from the vicinity of grain boundaries because of recoil energy from the transmutation. In this situation, Li in the HP304-CD specimens segregates in significant quantity to grain boundaries via a RIS process because the grain-boundary regions are relatively rich in Li. Lithium segregation in HP304-A was negligible apparently because the bulk concentration of B was lower (Table 9) and B did not segregate to grain boundaries (Fig. 29L).

#### 4.2.5 Grain-Boundary-Segregation-Transmutation (GST) Synergism: Effects of N and B

Based on the grain-boundary depletion and segregation behavior shown in Figs. 28-30 and the bulk chemical compositions given in Table 9, grain-boundary concentrations of alloying and impurity elements in the HP304-A and HP304-CD specimens have been calculated and plotted in Fig. 33. The grain-boundary concentrations were normalized in the plot to facilitate an easy comparison for the two materials, with actual numbers given for each of the elements. Figure 33 shows that grain-boundary concentrations of the two materials are virtually the same except for N, Li, and B. Grain-boundary concentrations of Cr, Ni, Si, P, C, and S are similar. Therefore, we conclude that higher concentration of N and lower concentrations of Li and B on grain boundaries are associated with the higher susceptibility of the HP304-A material to IGSCC during SSRT tests.

The exact mechanism by which higher N on grain boundaries promotes IGSCC is not clear. However, segregation of N will result in a higher concentration of hydrogen in a grain-boundary crack-tip region because of the transmutation of N to hydrogen (proton) by thermal neutrons, i.e., $^{14}N(n, p)^{14}C$. The cross section for this reaction is ≈1.83 barn. The mechanism whereby a higher Li concentration on grain boundaries is conducive to lower susceptibility to IGSCC is also not clear. Lithium, however, can trap hydrogen on grain boundaries.

The present study indicates that a synergism between grain-boundary segregation of impurities (N and B) and transmutation by thermal neutrons ("GST" synergism) plays an important role in IASCC. It also suggests that the relative importance of grain-boundary Cr depletion may be not as great as previously believed.

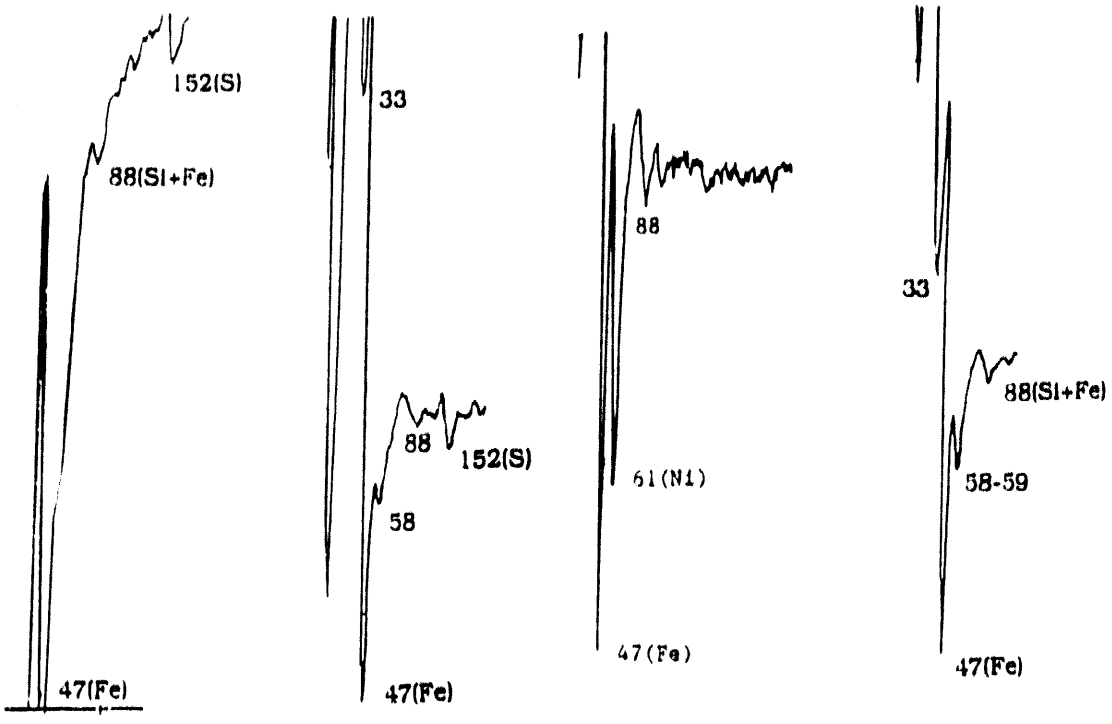

(A)
Unirradiated
CP 304 SS

(B)
Unirradiated
CP 304 SS
Corroded
in Li

(C)
Unirradiated
CP 310 SS

(D)
Irradiated
CP 304 SS
Grain Boundary

*Figure 31. Characteristic ≈59-eV Auger electron peaks obtained from several SSs; (A) nonirradiated CP Type 304; (B) Type 304 SS nonirradiated and corroded in liquid Li at 600°C for 144 h; (C) nonirradiated Type 310 SS containing ≈20 wt.% Ni; and (D) CP Type 304 SS irradiated to 2 x* $10^{21}$ n·cm$^{-2}$

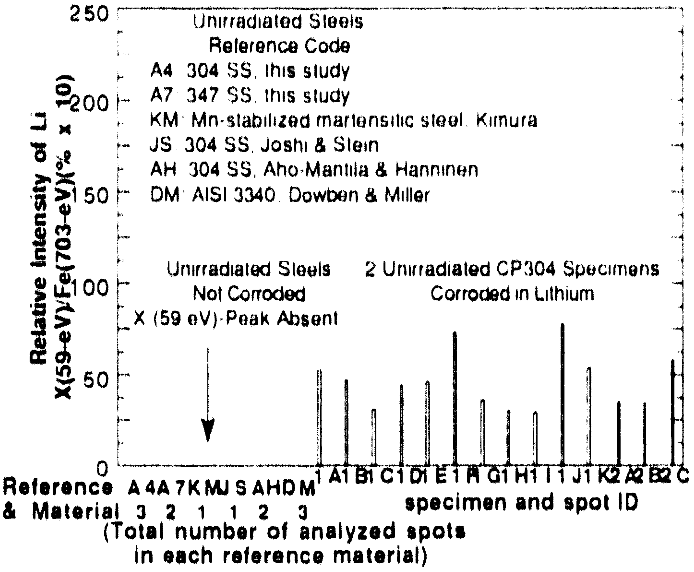

*Figure 32. Comparison of intensities of ≈59-eV Auger electron peak obtained from several types of nonirradiated steels either as-received or corroded in liquid Li at 600°C for 144 h*

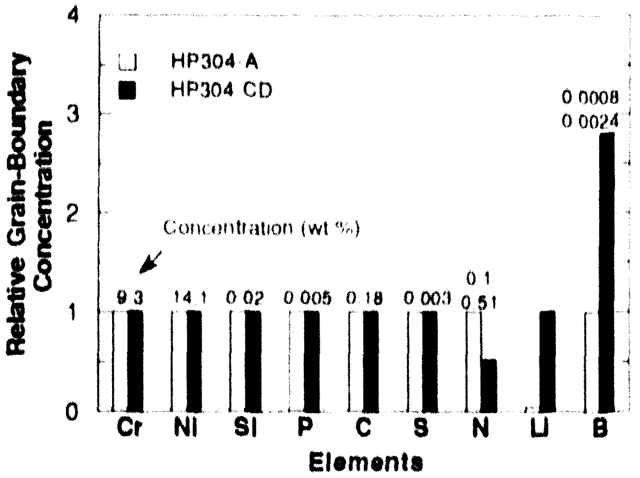

*Figure 33. Relative grain boundary concentrations of alloying and impurity elements in HP304 A and HP304 CD absorber tube specimens irradiated to ≈2 x $10^{21}$ n·cm$^{-2}$*

# 5 Environmentally Assisted Cracking of Ferritic Steels

Over the past 15 years, the corrosion fatigue properties of low alloy steels in LWR primary-system water chemistries have been studied extensively.$^{70-73}$ Much less information is available on SCC of these materials.$^{74-78}$ Because it is clear that very high CGRs can occur in some materials under some combinations of loading and environment, the objective of the current work is to better define the circumstances that can produce SCC in these steels.

## 5.1 Technical Progress (J. Y. Park)

Fracture-mechanics CGR tests have continued on 1T compact tension specimens from low- and medium-sulfur content heats (0.004 and 0.018 wt.%) of A533-Gr B pressure vessel steel and a medium-sulfur content (0.014%) A106-Gr B piping steel. One of the A533-Gr B specimens was Ni-Cr plated to better simulate a clad ferritic steel vessel, where only the low alloy steel at the crack surface is exposed to the environment. Surface films on the Ni-Cr and on Ni- and Au-plated specimens tested previously are different from those on the nonplated ferritic specimens. Because virtually all existing data have been obtained on specimens without cladding, it is important to verify that those results were not unduly affected by the character of the surface film.

CGR tests were conducted on a set of three carbon steel specimens [Nos. CTW7-03, 02C-14, and CTJ7-01] at a higher load ratio, i.e., R = 0.9. The composition of the steels was given in the previous report.$^{79}$ Specimens CTW7-03 and 02C-14 were prepared from plates of a low- and high-sulfur A533 Gr B pressure vessel steels, i.e., Heats No. A5401, (0.004% S and 0.005% P) and A-1195-1 (0.018% S and 0.012% P), respectively, and specimen CTJ7-01 was from a A106-Gr B piping steel, i.e., Heat No. J7201 (0.014% S and 0.014% P). Specimen 02C-14 was plated with Ni-Cr to simulate austenitic SS cladding on a reactor pressure vessel and hence, to determine the validity of using data obtained from specimens without cladding to analyze the behavior of a clad ferritic vessel where only the crack surface is exposed to the environment. In previous CGR tests, plated specimens showed greater susceptibility to SCC than did a conventional specimen under some loading conditions.[80]

Tests were performed in deionized water at 289°C under a cyclic load (sawtooth wave form with 12- and 1500-s loading and 1-s unloading time) at R = 0.9 and frequencies of $6.7 \times 10^{-4}$ and $7.7 \times 10^{-2}$ Hz. Initial $K_{max}$ values were 42, 104, and 33 $MPa \cdot m^{1/2}$ for specimens CTJ7-01, 02C-14, and CTW7-03, respectively. A DO concentration of 200-300 ppb in the effluent water from the autoclave was maintained by feedwater with 2-3 ppm DO. Crack length measurements were made by the DC potential drop method. The results of these and previous tests (Tests No. 1 to 38)[79] are summarized in Table 10. Crack growth occurred over a range of values from $4.4 \times 10^{-10}$ to $4.5 \times 10^{-8}$ $m \cdot s^{-1}$ for Specimen 02C-14, whereas no appreciable crack growth was observed for nonplated Specimens CTW7-03 and CTJ7-01. The CGRs for Specimen 02C-14 plotted as a function of maximum stress intensity in Figs. 34 and 35 are compared with rates predicted by the proposed ASME Code Section XI correlation.[81] The dependence of the CGRs on frequency for the plated specimen (02C-14) is shown in Fig. 36. All CGRs are bounded by the ASME code prediction. In previous tests[79] under different loading conditions (R = 0.2-0.7 and rise times in the range of 25-1500 s), some CGRs were faster than values predicted by the ASME correlation.

# 6 Summary of Results

## 6.1 Fatigue of Ferritic Piping and Pressure Vessel Steels

- The fatigue behavior of A106-Gr B carbon steel and A533-Gr B low alloy steel has been investigated in oxygenated water and in air. The results confirm the significant reduction in fatigue life and strong dependence on strain rate. For both carbon and low alloy steels, fatigue life in oxygenated water decreases with decreases in strain rate or increases in DO. The effects of strain rate on fatigue life saturate at some low value of strain rate, e.g., at 0.0004 %/s for A106-Gr B steel in water with ≈0.8 ppm DO. However, the results show that there is little difference in susceptibility to environmental degradation of fatigue life between A106-Gr B carbon steel and A533-Gr B low alloy steel with comparable sulfur levels.

## 6.2 Environmentally Assisted Cracking of Cast SS

- Additional crack growth tests have been conducted on fracture mechanics specimens of CF-8, and CF-8M grades of cast SS in the as-received and thermally aged conditions to characterize environmental, loading, and material conditions that can produce SCC susceptibility in these steels. CGRs in HP water containing 0.2 and 5-8 ppm DO were compared with predictions for wrought SS in air in Section XI of the ASME Code and modified correlations for wrought SSs in water. The results indicate that the air curve is frequently nonconservative, but the data are bounded by the modified correlations for wrought SSs in water at 289°C. Thermal aging increases the yield and ultimate strengths of the steels, and the CGRs in water tend to increase with the square of the yield stress.

*Table 10. Effect of frequency[a] on crack growth of A533-Gr B and A106-Gr B 1T-compact tension specimens[b] in 289°C water containing ≈200-300 ppb DO[c]*

| | | | Potentials | | Load | | Rise | A106-Gr B (No. CTJ7-01) Nonplated | | A533-Gr B (No. 02C-14) Ni-Cr Plated | | A533-Gr B (No. CTW7-03) Nonplated | |
|---|---|---|---|---|---|---|---|---|---|---|---|---|---|
| Test No. | Time, h | Cond., $\mu S \cdot cm^{-1}$ | A533, mV(SHE) | Pt | Ratio | Freq., $10^{-2}$ Hz | Time, s | $K_{max}$, $MPa \cdot m^{1/2}$ | Rate, $10^{-10}\ m \cdot s^{-1}$ | $K_{max}$, $MPa \cdot m^{1/2}$ | Rate, $10^{-10}\ m \cdot s^{-1}$ | $K_{max}$, $MPa \cdot m^{1/2}$ | Rate, $10^{-10}\ m \cdot s^{-1}$ |
| 1 | 1179<br>1212 | 0.08 | 153 | 231 | 0.2 | 7.7 | 12 | 25.5 | 0.7 | 21.3 | 51.5 | 22.5 | 0.3 |
| 2 | 1214<br>1220 | 0.08 | 159 | 231 | 0.2 | 3.9 | 25 | 25.5 | - | 21.4 | 53.8 | 22.5 | - |
| 3 | 1222<br>1229 | 0.08 | 138 | 227 | 0.2 | 2.0 | 50 | 25.5 | - | 21.6 | 36.4 | 22.4 | - |
| 4 | 1230<br>1242 | 0.08 | 154 | 238 | 0.2 | 1.0 | 100 | 25.5 | 3.2 | 21.7 | 29.1 | 22.4 | 1.1 |
| 5 | 1244<br>1252 | 0.08 | 181 | 239 | 0.2 | 0.5 | 200 | 25.5 | - | 21.9 | 26.9 | 22.4 | - |
| 6 | 1254<br>1262 | 0.09 | 187 | 251 | 0.2 | 0.25 | 400 | 25.5 | - | 21.9 | 20.8 | 22.4 | - |
| 7 | 1263<br>1272 | 0.07 | 183 | 250 | 0.2 | 0.13 | 750 | 25.5 | 3.1 | 22.0 | 7.9 | 22.4 | 1.5 |
| 8 | 1273<br>1322 | 0.08 | 159 | 237 | 0.2 | 0.07 | 1500 | 25.5 | - | 22.0 | 1.3 | 22.4 | - |
| 9 | 1324<br>1459 | 0.09 | 148 | 224 | 0.2 | 0.03 | 3000 | 25.5 | - | 22.1 | - | 22.5 | - |
| 10 | 1461<br>1484 | 0.10 | 153 | 222 | 0.2 | 3.9 | 25 | 25.6 | - | 22.2 | - | 22.5 | - |
| 11 | 1485<br>1490 | 0.10 | 146 | 221 | 0.2 | 7.7 | 12 | 25.6 | - | 22.3 | 59 | 22.5 | - |
| 12 | 1491<br>1508 | 0.10 | 141 | 225 | 0.7 | 7.7 | 12 | - | - | 22.5 | 11.0 | - | - |
| 13 | 1509<br>1522 | 0.07 | 138 | 223 | 0.7 | 3.9 | 25 | - | - | 22.6 | 9.9 | - | - |
| 14 | 1523<br>1584 | 0.07 | 129 | 205 | 0.7 | 2.0 | 50 | - | - | 22.6 | 0.4 | - | - |
| 15 | 1585<br>1606 | 0.10 | 141 | 234 | 0.7 | 1.0 | 100 | - | - | - | - | - | - |
| 16 | 1607<br>1628 | - | 127 | 225 | 0.7 | 7.7 | 12 | - | - | - | - | - | - |
| 17 | 1629<br>1634 | 0.11 | - | - | 0.2 | 7.7 | 12 | 22.5 | 0.7 | 22.6 | 63.2 | - | - |

*Table 10. (Cont'd)*

|  |  |  | Potentials |  | Load |  | Rise | A106-Gr B [No. CTJ7-01] Nonplated |  | A533-Gr B [No. 02C-14] Ni-Cr Plated |  | A533-Gr B [No. CTW7-03] Nonplated |  |
|---|---|---|---|---|---|---|---|---|---|---|---|---|---|
| Test No. | Time, h | Cond., $\mu S cm^{-1}$ | A533, mV(SHE) | Pt, mV(SHE) | Ratio | Freq., $10^{-2}$ Hz | Time, s | $K_{max}$, MPa m$^{1/2}$ | Rate, $10^{-10}$ m s$^{-1}$ | $K_{max}$, MPa m$^{1/2}$ | Rate, $10^{-10}$ m s$^{-1}$ | $K_{max}$, MPa m$^{1/2}$ | Rate, $10^{-10}$ m s$^{-1}$ |
| 18 | 1635<br>1642 | - | 139 | 228 | 0.5 | 7.7 | 12 | - | - | 23.0 | 71.3 | - | - |
| 19 | 1643<br>1650 | - | 139 | 228 | 0.5 | 3.9 | 25 | - | - | 23.2 | 72.1 | - | - |
| 20 | 1651<br>1656 | 0.07 | 131 | 221 | 0.5 | 2.0 | 50 | - | - | 23.4 | 55.6 | - | - |
| 21 | 1656<br>1663 | - | - | - | 0.5 | 1.0 | 100 | - | - | 23.4 | 15.4 | - | - |
| 22 | 1664<br>1685 | 0.08 | - | - | 0.5 | 0.5 | 200 | - | - | 23.5 | 5.3 | - | - |
| 23 | 1686<br>1948 | 0.07 | 153 | 213 | 0.5 | 0.25 | 400 | - | - | 23.5 | 0.2 | - | - |
| 24 | 1949<br>2278 | 0.07 | 186 | 239 | 0.5 | 0.13 | 750 | - | - | - | - | - | - |
| 25 | 2279<br>2284 | 0.10 | 154 | 218 | 0.2 | 7.7 | 12 | 29.9 | 27.8 | 29.3 | 458 | 26.6 | 70.1 |
| 26 | 2285<br>2290 | - | 167 | 233 | 0.2 | 3.9 | 25 | 30.2 | 54.2 | 31.1 | 388 | 26.8 | 50.0 |
| 27 | 2291<br>2294 | 0.11 | 152 | 214 | 0.2 | 2.0 | 50 | 30.4 | 70.8 | 32.3 | 276 | 26.9 | 52.8 |
| 28 | 2295<br>2298 | 0.11 | 152 | 214 | 0.2 | 1.0 | 100 | 30.6 | 41.7 | 33.0 | 253 | 27.0 | 51.4 |
| 29 | 2299<br>2302 | 0.11 | 158 | 213 | 0.2 | 0.5 | 200 | 30.7 | 47.2 | 33.8 | 243 | 27.0 | 9.7 |
| 30 | 2303<br>2306 | 0.06 | 144 | 191 | 0.2 | 0.25 | 400 | 30.8 | 33.3 | 34.5 | 229 | 27.0 | 6.9 |
| 31 | 2307<br>2312 | - | - | - | 0.2 | 0.13 | 750 | 30.9 | 16.7 | 35.3 | 140 | 27.0 | 1.4 |
| 32 | 2313<br>2318 | - | - | - | 0.2 | 0.07 | 1500 | 30.9 | 1.4 | 35.8 | 70.8 | - | - |
| 33 | 2319<br>2329 | 0.07 | - | - | 0.2 | 0.03 | 3000 | - | - | - | - | - | - |

*Table 10. (Cont'd)*

|  |  |  | Potentials |  | Load |  | Rise | A106-Gr B (No. CTJ7-01) Nonplated |  | A533-Gr B (No. 02C-14) Ni-Cr Plated |  | A533-Gr B (No. CTW7-03) Nonplated |  |
|---|---|---|---|---|---|---|---|---|---|---|---|---|---|
| Test No. | Time, h | Cond., µScm$^{-1}$ | A533, mV(SHE) | Pt. | Ratio | Freq., $10^{-2}$ Hz | Time, s | $K_{max}$, MPa m$^{1/2}$ | Rate, $10^{-10}$ m s$^{-1}$ | $K_{max}$, MPa m$^{1/2}$ | Rate, $10^{-10}$ m s$^{-1}$ | $K_{max}$, MPa m$^{1/2}$ | Rate, $10^{-10}$ m s$^{-1}$ |
| 34 | 4652<br>4657 | 0.08 | 124 | 197 | 0.2 | 7.7 | 12 | 38.8 | 429 | 46.2 | 885 | 32.7 | 82.6 |
| 35 | 4658<br>4661 | - | 109 | 193 | 0.2 | 3.9 | 25 | 39.8 | 211 | 51.7 | 908 | 33.1 | 90.3 |
| 36 | 4662<br>4665 | - | - | - | 0.2 | 2.0 | 50 | 40.05 | 182 | 59.3 | 510 | 33.1 | 26.4 |
| 37 | 4665<br>4668 | - | 113 | 190 | 0.2 | 1.0 | 100 | 41.2 | 190 | 76.0 | 2550 | 33.2 | 16.7 |
| 38 | 4669<br>4674 | 0.10 | 123 | 197 | 0.2 | 0.07 | 1500 | 41.5 | 30.5 | 103.6 | 1210 | 33.2 | - |
| 39 | 4675<br>4680 | 0.01 | 123 | 194 | 0.9 | 4.2 | 12 | - | - | 150.6 | 449 | - | - |
| 40 | 4681<br>4700 | 0.01 | 123 | 194 | 0.9 | 3.9 | 25 | - | - | 172.2 | 72 | - | - |
| 41 | 4701<br>4726 | 0.12 | 123 | 196 | 0.9 | 2.0 | 50 | - | - | 180.6 | 28.7 | - | - |
| 42 | 4727<br>4780 | - | 122 | 195 | 0.9 | 1.0 | 100 | - | - | 189.8 | 13.5 | - | - |
| 43 | 4781<br>4820 | 0.09 | 145 | 218 | 0.9 | 0.5 | 200 | - | - | 196.6 | 19.9 | - | - |
| 44 | 4821<br>4916 | 0.11 | 132 | 204 | 0.9 | 0.25 | 400 | - | - | 203.9 | 4.4 | - | - |
| 45 | 4917<br>5060 | 0.07 | 140 | 206 | 0.9 | 0.13 | 750 | - | - | 217.3 | 5.6 | - | - |
| 46 | 5061<br>5133 | 0.09 | 144 | 221 | 0.9 | 0.07 | 1500 | - | - | 244.1 | 19.5 | - | - |

[a] Positive sawtooth wave form was used.

[b] Heats No. J7201 for A106 Gr-B (Specimen No. CTJ7-01), A-1195-1 for A533-Gr B (Specimen No. 02C-14) and A5401 for A533-Gr B (Specimen No. CTW7-03). Crack plane orientation was the L-T direction.

[c] Effluent dissolved-oxygen concentration was ~200-300 ppb; feedwater oxygen concentration was approximately an order of magnitude higher to compensate for oxygen depletion by corrosion of the autoclave system.

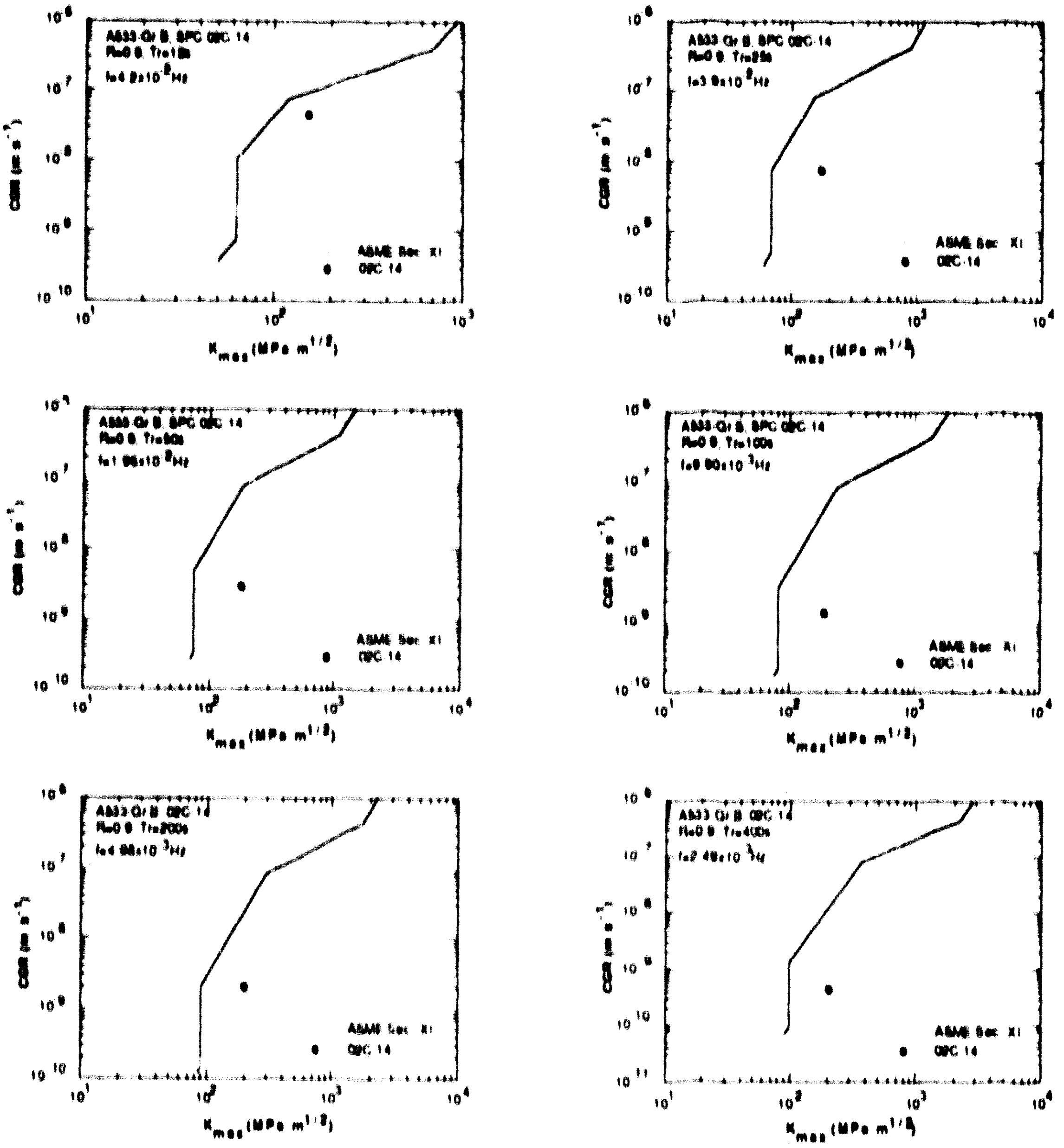

*Figure 34. Crack growth rates vs. maximum stress intensity for Cr-Ni plated A533-Gr B (0.018% S, 02C-14) steel in HP oxygenated water at 289°C at rise times of 12-400 s at R = 0.9*

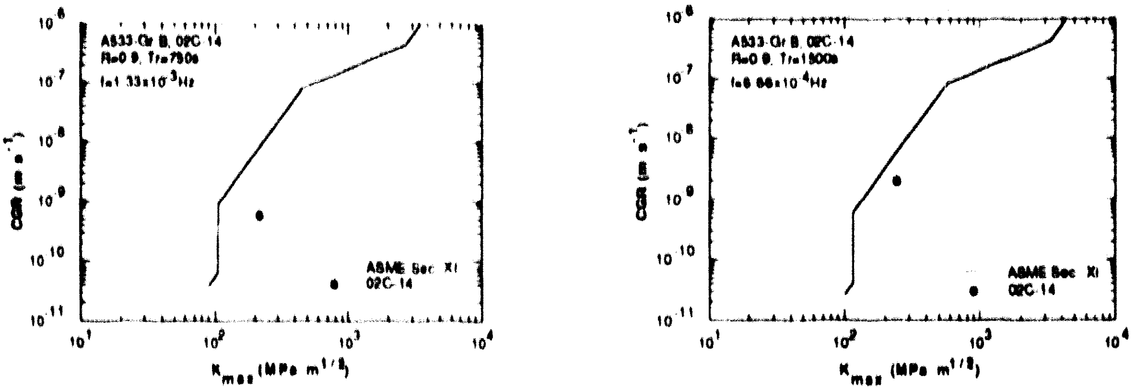

*Figure 35. Crack growth rates vs. maximum stress intensity for Cr–Ni plated A533-Gr B (0.018% S, 02C-14) steel in HP oxygenated water at 289°C at rise times of 75 and 1500 s at R = 0.9*

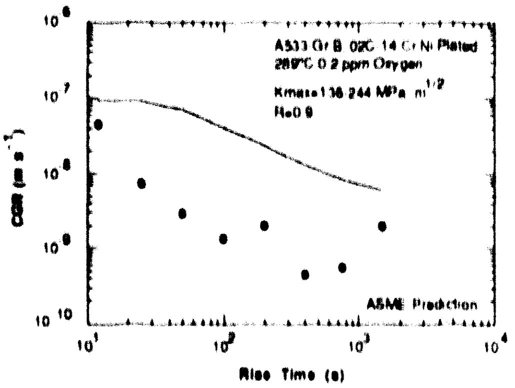

*Figure 36. Crack growth rates vs. rise time for Cr–Ni plated A533-Gr B steel (0.018% S) at R = 0.9 in HP oxygenated water at 289°C*

## 6.3 Irradiation–Assisted Stress Corrosion Cracking of Type 304 SS

- SSRT tests and grain-boundary analysis by AES were conducted on high- and commercial-purity (HP and CP) Type 304 SS specimens from irradiated BWR components. Contrary to previous beliefs, susceptibility to IGSCC could not be correlated with radiation-induced segregation (RIS) of impurities such as Si, P, C, or S, but a correlation was obtained with grain-boundary Cr concentration, indicating a role of Cr depletion. However, grain-boundary concentrations of Cr determined from presently available FEG-STEM-EDS and AES techniques are not accurate enough to clarify the importance of the role of Cr depletion.

- Grain-boundary analysis was conducted on BWR neutron absorber tubes that were fabricated from two HP heats of Type 304 SS that had virtually identical chemical compositions and that were irradiated to similar fluence level but exhibited a significant difference in susceptibility to IGSCC during SSRT tests. Grain-boundary concentrations of Cr, Ni, Si, P, S, and C of the resistant and susceptible heats were virtually identical. However, grain boundaries of the resistant material contained a lower concentration of N and higher concentrations of B and Li than those of the susceptible material.

- Boron is known to undergo thermal segregation to grain boundaries in austenitic SSs. Therefore, grain-boundary concentrations of B, and hence Li, could be influenced strongly by thermomechanical processes even if core-internal components are fabricated from the same starting material. In slow cooling of thicker sections (e.g., BWR top guide), thermal segregation of B, and hence Li, is likely to be more pronounced. This will be conducive to the suppression of IASCC under conditions of similar thermal sensitization (i.e., Cr depletion).

- The present study indicates that a synergism between grain-boundary segregation of N and B impurities and transmutation by thermal neutrons to H and Li, respectively, ("GST" synergism) plays an important role in IASCC. However, the relative importance of the roles of grain-boundary Cr depletion and the "GST" synergism is not clear.

### 6.4 Environmentally Assisted Cracking of Ferritic Steels

- Additional fracture-mechanics CGR tests have been performed on nonplated specimens of A106-Gr B and A533-Gr B steel and on a specimen of A533-Gr B plated with Ni-Cr. The effect of frequency on CGR was determined at a load ratio of 0.9 in HP oxygenated (≈200 ppb) water at 289°C. The CGRs for the Ni-Cr-plated A533-Gr B specimen were compared with predicted values from new correlations proposed for inclusion in Section XI of the ASME Boiler and Pressure Vessel Code. The observed CGRs were adequately bounded by the proposed ASME Section XI correlations.

## Acknowledgments

W. F. Burke, G. Dragel, D. R. Perkins, D. A. Donahue, and J. C. Tezak contributed to the experimental effort in this program. The BWR components were obtained through the kind assistance of Dr. A. J. Jacobs of General Electric Company. This work was part of a program entitled "Environmentally Assisted Cracking in LWR Systems," sponsored by the Office of Nuclear Regulatory Research, U.S. Nuclear Regulatory Commission, under FIN Number A2212; Program Manager: Dr. J. Muscara.

## References

1. K. Iida, A Review of Fatigue Failures in LWR Plants in Japan, *Nucl. Eng. Des.* **138**, 297-312 (1992).
2. *Criteria of Section III of the ASME Boiler and Pressure Vessel Code for Nuclear Vessels*, The American Society of Mechanical Engineers, United Engineering Center, New York, Library of Congress Catalog No. 56-3934 (1989).
3. *Tentative Structural Design Basis for Reactor Pressure Vessels and Directly Associated Components (Pressurized, Water Cooled Systems)*, PB 151987, U.S. Department of Commerce, Office of Technical Service, 1 Dec. 1958 Revision.
4. D. A. Hale, S. A. Wilson, E. Kiss, and A. J. Gianuzzi, *Low Cycle Fatigue Evaluation of Primary Piping Materials in a BWR Environment*, GEAP-20244, U.S. Nuclear Regulatory Commission (Sept. 1977).

5. D. A. Hale, S. A. Wilson, J. N. Kass, and E. Kiss, Low Cycle Fatigue Behavior of Commercial Piping Materials in a BWR Environment, *J. Eng. Mater. Technol.* **103**, 15–25 (1981).

6. S. Ranganath, J. N. Kass, and J. D. Heald, "Fatigue Behavior of Carbon Steel Components in High-Temperature Water Environments," *Low-Cycle Fatigue and Life Prediction*, ASTM STP 770, C. Amzallag, B. N. Leis, and P. Rabbe, eds., American Society for Testing and Materials, Philadelphia, PA, pp. 436–459 (1982).

7. J. B. Terrell, *Fatigue Life Characterization of Smooth and Notched Piping Steel Specimens in 288°C Air Environments*, NUREG/CR-5013, MEA-2232 (May 1988).

8. J. B. Terrell, Effect of Cyclic Frequency on the Fatigue Life of ASME SA-106-B Piping Steel in PWR Environments, *J. Mater. Eng.* **10**, 193–203 (1988).

9. P. D. Hicks, in *Environmentally Assisted Cracking in Light Water Reactors: Semiannual Report October 1990—March 1991*, NUREG/CR-4667 Vol. 12, ANL-91/24, pp. 3–18 (Aug. 1991).

10. P. D. Hicks and W. J. Shack, Fatigue of Ferritic Steels, in *Environmentally Assisted Cracking in Light Water Reactors, Semiannual Report, April–September 1991*, NUREG/CR-4667 Vol. 13, ANL-92/6, pp. 3–8 (March 1992).

11. M. Higuchi and K. Iida, Fatigue Strength Correction Factors for Carbon and Low-Alloy Steels in Oxygen-Containing High-Temperature Water, *Nucl. Eng. Des.* **129**, 293–306 (1991).

12. K. Iida, H. Kobayashi, and M. Higuchi, *Predictive Method of Low Cycle Fatigue Life of Carbon and Low Alloy Steels in High Temperature Water Environments*, NUREG/CP-0067, MEA-2090, Vol. 2 (April 1986).

13. N. Nagata, S. Sato, and Y. Katada, Low-Cycle Fatigue Behavior of Low-Alloy Steels in High-Temperature Pressurized Water, *Transactions of the 10th International Conf. on Structural Mechanics in Reactor Technology*, Vol. F, A. H. Hadjian, ed., American Association for Structural Mechanics in Reactor Technology, Anaheim, CA (1989).

14. S. Majumdar, O. K. Chopra, and W. J. Shack, *Interim Fatigue Design Curves for Carbon, Low-Alloy, and Austenitic Stainless Steels in LWR Environments*, NUREG/CR-5999, ANL-93/3 (April 1993).

15. T. A. Prater and L. F. Coffin, *The Use of Notched Compact-Type Specimens for Crack Initiation Design Rules in High-Temperature Water Environments*, Corrosion Fatigue: Mechanics Metallurgy, Electrochemistry, and Engineering, ASTM STP 801, T. W. Crooker and B. N. Leis, eds., American Society for Testing and Materials, Philadelphia, pp. 423-444 (1983).

16. T. A. Prater and L. F. Coffin, *Notch Fatigue Crack Initiation in High Temperature Water Environments: Experiments and Life Prediction*, J. of Pressure Vessel Technol., Trans. ASME, **109**, 124–134 (1987).

17. O. K. Chopra and G. Ayrault, *Aging Degradation of Cast Stainless Steel: Status and Program*, Nucl. Eng. Des. **86**, 69-77 (1985).

18. H. M. Chung and O. K. Chopra, *Microstructures of Cast-Duplex Stainless Steels After Long-Term Aging*, in Proc. of the 2nd Int. Symp. on Environmental Degradation of Materials in Nuclear Power Systems - Water Reactors, Monterey, CA, The American Nuclear Society, La Grange Park, IL, pp. 287-292 (1986).

19. H. M. Chung and O. K. Chopra, *Long-Term Aging Embrittlement of Cast Austenitic Stainless Steels - Mechanisms and Kinetics*, in Properties of Stainless Steels in Elevated Temperature Service, M. Prager, ed., MPC-Vol. 26, PVP Vol. 132, American Society of Mechanical Engineers, New York, pp. 17-34 (1988).

20. H. M. Chung and O. K. Chopra, *Kinetics And Mechanisms of Thermal Aging Embrittlement of Duplex Stainless Steels*, in Proc. 3rd Int. Symp. on Environmental Degradation of Materials in Nuclear Power Systems - Water Reactors, Traverse City, MI, G. J. Theus and J. R. Weeks, eds., The Metallurgical Society, pp. 359-370 (1988).

21. H. M. Chung, *Thermal Aging of Decommissioned Reactor Cast Stainless Steel Components and Methodology for Life Prediction*, Proc. 1989 ASME Pressure Vessel and Piping Conf., Honolulu, Hawaii, T. V. Narayana, et. al., eds., PVP Vol. 171, pp. 111-115 (1989).

22. H. M. Chung, *Spinodal-like Decomposition of Austenite in Long-Term Aged Duplex Stainless Steel*, Physical Metallurgy of Controlled Expansion Invar-Type Alloys, K. C. Russell and D. F. Smith, eds., The Minerals, Metals, and Materials Society, Warrendale, PA, pp. 129-141 (1990).

23. H. M. Chung and T. R. Leax, *Embrittlement of Laboratory- and Reactor-Aged CF-3, CF-8, and CF-8M Duplex Stainless Steels*, Mater. Sci. and Technol. **6**, 249-262 (1990).

24. H. M. Chung and O. K. Chopra, *Accelerated Aging Embrittlement of Cast Duplex Stainless Steel - Activation Energy for Extrapolation*, Proc. 4th Int. Symp. on Environmental Degradation of Materials in Nuclear Power Systems - Water Reactors, D. Cubicciotti, ed., National Association of Corrosion Engineers, Houston, pp. 3-47 to 3-65 (1990).

25. H. M. Chung, *Evaluation and Diagnosis of Aging of Cast Stainless Steel Components*, Proc. ASME Pressure Vessel and Piping Conf., PVP Vol. 208, American Society of Mechanical Engineers, New York, pp. 121-136 (1991).

26. H. M. Chung, *Aging and Life Prediction of Cast Duplex Stainless Steel Components*, Int. J. Pres. Ves. & Piping **50**, 179-213 (1992).

27. O. K. Chopra and H. M. Chung, *Aging of Cast Duplex Stainless Steels in LWR Systems*, Nucl. Eng. Des. **89**, 305-318 (1985).

28. O. K. Chopra and H. M. Chung, *Effects of Low Temperature Aging on the Mechanical Properties of Cast Stainless Steels*, in Properties of Stainless Steels in Elevated Temperature Service, M. Prager, ed., MPC-Vol. 26, PVP Vol. 132, American Society of Mechanical Engineers, New York, pp. 79-105 (1988).

29. O. K. Chopra and H. M. Chung, *Aging Degradation of Cast Stainless Steels: Effects on Mechanical Properties*, in Proc. 3rd Int. Symp. on Environmental Degradation of Materials in Nuclear Power Systems - Water Reactors, Traverse City, MI, G. J. Theus and J. R. Weeks, eds., The Metallurgical Society, pp. 737-748 (1988).

30. O. K. Chopra and H. M. Chung, *Embrittlement of Cast Stainless Steels in LWR Systems*, Proc. 15th MPA Seminar on Safety and Reliability of Plant Technology, Vol. 1, pp. 13.1-13.23 (1989).

31. O. K. Chopra, *Thermal Aging of Cast Stainless Steels: Mechanisms and Predictions*, Fatigue, Degradation, and Fractures, W. H. Bamford, C. Becht IV, S. Bhandari, J. D. Gilman, L. A. James, and M. Prager, eds., PVP Vol. 195, The American Society of Mechanical Engineers, New York, pp. 193-214 (1990).

32. O. K. Chopra, *Thermal Aging of Cast Stainless Steels in LWR Systems: Estimation of Mechanical-Properties*, Nuclear Plant Systems/Components Aging Management and Life Extension, American Society of Mechanical Engineers, PVP Vol. 228, pp. 79–92 (1992).

33. O. K. Chopra, *Prediction of Aging Degradation of Cast Stainless Steel Components in LWR Systems*, in Proc. Aging Research Information Conf., NUREG/CP-0122 Vol. 2, pp. 324–340 (1992).

34. O. K. Chopra and W. J. Shack, *Evaluation of Aging Degradation of Structural Components*, in Proc. Aging Research Information Conf., NUREG/CP-0122 Vol. 2, pp. 369–386 (1992).

35. O. K. Chopra, *Long-Term Embrittlement of Cast Duplex Stainless Steels in LWR Systems: Semiannual Report, October 1990 - March 1991*, NUREG/CR-4744 Vol. 6, No 1, ANL-91/22 (Aug. 1992).

36. O. K. Chopra, *Long-Term Embrittlement of Cast Duplex Stainless Steels in LWR Systems: Semiannual Report, April - September 1991*, NUREG/CR-4744 Vol. 6, No 2, ANL-92/32 (Nov. 1992).

37. O. K. Chopra, *Long-Term Embrittlement of Cast Duplex Stainless Steels in LWR Systems: Semiannual Report, October 1991 - March 1992*, NUREG/CR-4744 Vol. 7, No 1, ANL-92/42 (May 1993).

38. W. E. Ruther, O. K. Chopra, and T. F. Kassner, in *Environmentally Assisted Cracking in Light Water Reactors: Semiannual Report, April - September 1992*, NUREG/CR-4667 Vol. 15, ANL-93/2, pp. 21-28 (June 1993).

39. W. E. Ruther, J. Y. Park, T. F. Kassner, and W. K. Soppet, in *Environmentally Assisted Cracking in Light Water Reactors: Semiannual Report, October 1988 - March 1989* NUREG/CR-4667 Vol. 8, ANL-90/4, pp. 2-5 (June 1990).

40. J. Y. Park and W. J. Shack, in *Environmentally Assisted Cracking in Light Water Reactors: Semiannual Report, April 1989 - September 1989*, NUREG/CR-4667 Vol. 9, ANL-90/48, pp. 3-6 (March 1991).

41. W. J. Shack, in *Environmentally Assisted Cracking in Light Water Reactors: Semiannual Report, October 1990 - March 1991*, NUREG/CR-4667 Vol. 12, ANL-91/24, pp. 30–37 (Aug. 1991).

42. A. B. Hull, P. R. Luebbers, M. R. Fox, W. K. Soppet, and T. F. Kassner, *Aqueous Stress Corrosion of Candidate Austenitic Stainless Steels for ITER Applications, in Fusion Reactor Materials Semiannual Progress Report for the Period Ending March 31, 1992*, DOE/ER-0313/12, pp. 225–235 (July 1992).

43. D. M. French, W. K. Soppet, and T. F. Kassner, *Aqueous Stress Corrosion of Candidate Austenitic Stainless Steels for ITER Applications, in Fusion Reactor Materials Semiannual Progress Report for the Period Ending September 30, 1992*, DOE/ER-0313/13, pp. 276–284 (March 1993).

44. W. E. Ruther, T. F. Kassner and J. Y. Park, in *Environmentally Assisted Cracking in Light Water Reactors: Semiannual Report, October 1991 - March 1992*, NUREG/CR-4667 Vol. 14, ANL-92/30, pp. 33-42 (Aug. 1992).

45. X. J. Wu, A. K. Koul, and A. S. Krqusz, *A Transgranular Fatigue Crack Growth Model Based on Restricted Slip Reversibility*, Met Trans. **24A**, 1373-1380 (1993).

46. J. F. Knott, *Fundamentals of Fracture Mechanics*, John Wiley & Sons, New York (1973).

47. J. P. Benson and D. V. Edmonds, Met. Sci. **12**, 223-232 (1978).

48. J. Low, U. Wolff, and W. Cowden, *Electron Microscopic Examination of Failed Stainless Steel Fuel Cladding - Dresden Advanced Fuel Assemblies PF-1 and PR-4*, APED-4242, General Electric Co. (May 1965).

49. J. S. Armijo, *Effect of Impurity Additions on the Intergranular Corrosion of High Purity Fe-Cr-Ni Austenitic Alloys, GEAP-5047*, General Electric Co. (Oct. 1966).

50. J. S. Armijo, *Grain Boundary Studies of Austenitic Stainless Steels*, GEAP-5503, General Electric Co. (Sept. 1967).

51. J. S. Armijo, *Intergranular Corrosion of Nonsensitized Austenitic Stainless Steels*, Corrosion **24**, 24-30 (1968).

52. R. Duncan, *Stainless Steel Failure Investigation Program*, GEAP-5530, General Electric Co. (Feb. 1968).

53. A. Strasser, J. Santucci, K. Lindquist, W. Yario, G. Stern, L. Goldstein, and L. Joseph, *Evaluation of Stainless Steel Cladding in LWRs*, EPRI NP-2642, Electric Power Research Institute, Palo Alto, CA (Dec. 1982).

54. F. Garzarolli, D. Alter, and P. Dewes, *Deformability of Austenitic Stainless Steels and Ni-Base Alloys in the Core of a Boiling and Pressurized Water Reactor*, Proc. 2nd Int. Symp. Environmental Degradation of Materials in Nuclear Power Systems - Water Reactors, National Association of Corrosion Engineers, Houston, pp. 131-138 (1986).

55. F. Garzarolli, D. Alter, P. Dewes, and J. L. Nelson, *Deformability of Austenitic Stainless Steels and Ni-Base Alloys in the Core of a Boiling and Pressurized Water Reactor*, Proc. 3rd Int. Symp. Environmental Degradation of Materials in Nuclear Power Systems - Water Reactors, G. J. Theus and J. R. Weeks, eds., The Metallurgical Society, Warrendale, PA, pp. 657-664 (1988).

56. A. J. Jacobs, R. E. Clausing, M. K. Miller, and C. Shepherd, *Influence of Grain Boundary Composition on the IASCC Susceptibility of Type 348 Stainless Steel*, Proc. 4th Int. Symp. Environmental Degradation of Materials in Nuclear Power Systems - Water Reactors, National Association of Corrosion Engineers, Houston, pp. 14-21 to 14-45 (1990).

57. A. J. Jacobs, G. P. Wozaldo, K. Nakata, T. Yoshida, and I. Masaoka, *Radiation Effects on the Stress Corrosion and Other Selected Properties of Type-304 and Type-316 Stainless Steels*, Proc. 3rd Int. Symp. Environmental Degradation of Materials in Nuclear Power Systems - Water Reactors, G. J. Theus and J. R. Weeks, eds., The Metallurgical Society, Warrendale, PA, pp. pp. 673-681 (1988).

58. A. J. Jacobs, *The Relationship of Grain Boundary Composition in Irradiated Type 304 SS to Neutron Fluence and IASCC*, Effects of Radiation on Materials: 16th Int. Symp., ASTM STP 1175, A. S. Kumar, D. S. Gelles, R. K. Nanstad, and T. A. Little, eds., American Society for Testing and Materials, Philadelphia, 1993.

59. H. M. Chung, W. E. Ruther, J. E. Sanecki, A. G. Hins, and T. F. Kassner, *Stress Corrosion Cracking Susceptibility of Irradiated Type 304 Stainless Steels*, Effects of Radiation on Materials: 16th Int. Symp., ASTM STP 1175, A. S. Kumar, D. S. Gelles, R. K. Nanstad, and T. A. Little, eds., American Society for Testing and Materials, Philadelphia, 1993.

60. H. M. Chung, W. E. Ruther, J. E. Sanecki, and A. G. Hins, in *Environmentally Assisted Cracking in Light Water Reactors: Semiannual Report April-September 1992*, NUREG/CR-4667, Vol. 15, ANL-93/2, Argonne National Laboratory, pp. 28-60 (June 1993).

61. K. Fukuya, S. Shima, H. Kayano, and M. Narui, *Stress Corrosion Cracking and Intergranular Corrosion of Neutron Irradiated Austenitic Steels*, J. Nucl. Mater. **191-194**, 1007-1011 (1992).

62. K. Fukuya, K. Nakata, and A. Horie, *An IASCC Study Using High Energy Ion Irradiation*, Proc. 5th Int. Symp. Environmental Degradation of Materials in Nuclear Power Systems - Water Reactors, American Nuclear Society, La Grange Park, IL, pp. 814-820 (1992).

63. J. M. Cookson, R. D. Carter, D. L. Damcott, M. Atzmon, G. S. Was, and P. L. Andresen, *Stress Corrosion Cracking of High Energy Proton-Irradiated Stainless Steels*, ibid., pp. 806-813.

64. M. Kodama, S. Nishimura, J. Morisawa, S. Shima, S. Suzuki, and M. Yamamoto, *Effects of Fluence and Dissolved Oxygen on IASCC in Austenitic Stainless Steels*, Proc. 5th Int. Symp. Environmental Degradation of Materials in Nuclear Power Systems - Water Reactors, American Nuclear Society, La Grange Park, IL, pp. 948-954 (1992).

65. K. Asano, K. Fukuya, K. Nakata, and K. Kodama, *Changes in Grain Boundary Composition by Neutron Irradiation on Austenitic Stainless Steels*, ibid. pp. 838-843.

66. E. A. Kenik, *Radiation-Induced Segregation in Irradiated Type 304 Stainless Steels*, J. Nucl. Mater. **187** (1992), 239-246.

67. S. M. Bruemmer, B. W. Arey, and L. A. Charlot, *Influence of Chromium Depletion on the Intergranular Stress Corrosion Cracking of 304 Stainless Steel*, Corrosion **48**(1), 42-49 (1992).

68. D. I. R. Norris, C. Baker, and J. M. Titchmarsh, *Compositional Profiles at Grain Boundaries in 20%Cr/25%Ni/Nb Stainless Steel*, Proc. Symp. on Radiation-Induced Sensitization of Stainless Steels, D. I. R. Norris, ed., Central Electricity Generating Board, Berkeley, England, pp. 86-98 (1987).

69. J. M. Titchmarsh and I. A. Vatter, *Measurement of Radiation-Induced Segregation Profiles by High Spatial Resolution Electron Microscopy*, ibid., pp. 74-85.

70. P. D. Hicks and F. P. A. Robinson, *Fatigue Crack Growth Rates in a Pressure Vessel Steel under Various Conditions of Loading and the Environment*, Met. Trans. **17A**, 1837-1849 (1986).

71. *Proc. of Int. Atomic Energy Agency Specialists' Meeting on Subcritical Crack Growth*, NUREG/CP-0044, MEA-2014, Vols. 1 & 2 (May 1983).

72. *Proc. of 2nd Int. Atomic Energy Agency Specialists' Meeting on Subcritical Crack Growth*, NUREG/CP-0067, MEA-2090, Vols. 1 & 2 (April 1986).

73. *Proc. of 3rd Int. Atomic Energy Agency Specialists' Meeting on Subcritical Crack Growth*, NUREG/CP-0112, Vols. 1 & 2 (Aug. 1990).

74. T. A. Prater, W. R. Catlin, and L. F. Coffin, *Surface Crack Growth Behavior of Structural Metals in High Temperature Water Environments*, J. Eng. Mater. Technol. **108**, 2-9 (1986).

75. M. O. Speidel and R. M. Magdowski, *Stress Corrosion Cracking of Nuclear Reactor Pressure Vessel Steel in Water: Crack Initiation versus Crack Growth*, NACE Corrosion 88, Paper No. 283, St. Louis, MO, (Mar. 1988).

76. D. A. Hale, *The Effect of BWR Startup Environments on Crack Growth in Structural Alloys*, J. Eng. Mater. Technol. **108**, 44-49 (1986).

77. F. P. Ford and P. L. Andresen, *Stress Corrosion Cracking of Low-Alloy Pressure Vessel Steels in 288°C Water*, in Proc. 3rd Int. Atomic Energy Agency Specialists' Meeting on Subcritical Crack Growth, NUREG/CP-0112, Vol. 1, pp. 37-56 (Aug. 1990).

78. P. M. Scott and D. R. Tice, *Stress Corrosion in Low-Alloy Steels*, Nucl. Eng. Des. **119**, 399-413 (1990).

79. J. Y. Park, in *Environmentally Assisted Cracking in Light Water Reactors: Semiannual Report April —September 1992*, NUREG/CR-4667 Vol. 15, ANL-93/2, pp. 13-20 (June 1993).

80. J. Y. Park, in *Environmentally Assisted Cracking in Light Water Reactors: Semiannual Report October 1991—March 1992*, NUREG/CR-4667 Vol. 14, ANL-92/30, pp. 14-18 (Aug. 1992).

81. E. D. Eason, *EDEAC Status; Analysis Procedures for da/dN and S-N Data*, in Technical Information from Workshop Cyclic Life and Environmental Effects in Nuclear Applications, Vol. 2, Clearwater Beach, FL, Pressure Vessel Research Committee and Welding Research Council (Jan. 20-21, 1992).

## Distribution for NUREG/CR-4667, Vol. 16 (ANL-93/27)

Internal

W. J. Shack (45)

TIS Files

External

NRC for distribution per R5

Libraries

- ANL-E
- ANL-W

Manager, Chicago Field Office, DOE

Energy Technology Division Review Committee:

- H. K. Birnbaum, University of Illinois, Urbana
- R. C. Buchanan, University of Cincinnati, Cincinnati
- M. S. Dresselhaus, Massachusetts Institute of Technology, Cambridge, MA
- B. G. Jones, University of Illinois, Urbana
- C.-Y. Li, Cornell University, Ithaca, NY
- S. N. Liu, Fremont, CA
- R. E. Smith, Engineering Applied Sciences, Inc., Trafford, PA

P. L. Andresen, General Electric Corporate Research and Development, Schenectady, NY

R. G. Ballinger, Massachusetts Institute of Technology, Cambridge, MA

W. H. Bamford, Structural Materials Engineering, Westinghouse Electric Corp., Pittsburgh

S. M. Bruemmer, Battelle Pacific Northwest Laboratory

G. Cragnolino, Southwest Research Inst., San Antonio, TX

W. H. Cullen, Materials Engineering Assoc., Inc., Lanham, MD

R. Duncan, ABB CE Nuclear Power, Windsor, CT

E. D. Eason, Modeling and Computing Services, Newark, CA

M. Fox, APTECH, Tucson, AZ

D. G. Franklin, Bettis Atomic Power Laboratory

Y. S. Garud, S. Levy, Inc., Campbell, CA

F. Garzarolli, KWU, Erlangen, Germany

J. Gilman, Electric Power Research Inst., Palo Alto, CA

B. M. Gordon, General Electric Co., San Jose, CA

S. J. Green, Electric Power Research Institute, Palo Alto, CA

J. W. Halley, U. Minnesota, Minneapolis

H. E. Hanninen, Technical Research Centre of Finland, Espoo

D. Harrison, USDOE, Germantown, MD

J. Hickling, CML Capcis March Ltd., Erlangen-Tennonlohe, Germany

C. Hoffmann, ABB CE Nuclear Power, Windsor, CT

M. E. Indig, General Electric Co., Pleasanton, CA

H. S. Isaacs, Brookhaven National Laboratory

A. Jacobs, General Electric Co., San Jose, CA

L. James, Bettis Atomic Power Laboratory

C. Jansson, Vattenfall Energisystem, Vallingby, Sweden

R. H. Jones, Battelle Pacific Northwest Laboratory

T. Karlsen, OECD Halden Reactor Project, Halden, Norway

J. N. Kass, Lawrence Livermore National Laboratory

C. Kim, Westinghouse Electric Corp., Pittsburgh

L. Ljungberg, ASEA-ATOM, Vasteras, Sweden

C. D. Lundin, U. Tennessee, Knoxville

D. D. Macdonald, Pennsylvania State University, University Park

T. R. Mager, Westinghouse Electric Corp., Pittsburgh

H. Metha, General Electric Co., San Jose, CA

D. Morgan, Pennsylvania Power and Light Co., Allentown, PA

J. L. Nelson, Electric Power Research Inst., Palo Alto, CA

M. Prager, Materials Properties Council, New York, NY

S. Ranganath, General Electric Co., San Jose, CA

P. M. Scott, Framatome, Paris, France

C. Shepherd, AEA Technology Harwell Labs., Didcot, Oxon, UK

S. Smialowska, Ohio State University, Columbus

M. O. Speidel, Swiss Federal Institute of Technology, Zurich, Switzerland

D. M. Stevens, Lynchburg Research Center, Babcock & Wilcox Co., Lynchburg, VA

W. A. Van Der Sluys, Research & Development Division, Babcock & Wilcox Co., Alliance, OH

J. C. Van Duysen, Electricite de France Research and Development Centre de Renardieres, Moret-Sur-Loing, France

E. Venerus, Knolls Atomic Power Laboratory

J. R. Weeks, Brookhaven National Laboratory

D. Winkel, Teleco Oil Field Services, Meriden, CT

S. Yukewa, Boulder, CO

# DATE FILMED

11/22/93

# END